HHS Public Access

Author manuscript

Circulation. Author manuscript; available in PMC 2021 November 17.

Published in final edited form as:

Circulation. 2020 November 17; 142(20): 1937–1955. doi:10.1161/CIRCULATIONAHA.120.046450.

Complex Arrhythmia Syndrome in a Knock-In Mouse Model Carrier of the N98S *Calm1* Mutation

Wen-Chin Tsai, MD, PhD[1,2,*], **Shuai Guo, MD**[1,3,*], **Michael A. Olaopa, PhD**[1], **Loren J. Field, PhD**[1,4], **Jin Yang, PhD**[1], **Changyu Shen, PhD**[5], **Ching-Pin Chang, MD, PhD**[1], **Peng-Sheng Chen, MD**[1,#], **Michael Rubart, MD**[1,4,#]

[1]The Krannert Institute of Cardiology and Division of Cardiology, Department of Medicine, Indiana University School of Medicine, Indianapolis, IN, USA

[2]Department of Cardiology, Cardiovascular Research Center, Buddhist Tzu Chi General Hospital and Tzu Chi University, Hualien, Taiwan

[3]Department of Cardiology, The First Affiliated Hospital of Harbin Medical University, Harbin, China

[4]Wells Center for Pediatric Research, Department of Pediatrics, Indiana University School of Medicine, Indianapolis, IN, USA

[5]Beth Israel Deaconess Medical Center, Harvard Medical School, Boston, MA, USA

Abstract

Background: Calmodulin mutations are associated with arrhythmia syndromes in humans. Exome sequencing previously identified a *de novo* mutation in *CALM1* resulting in a p.N98S substitution in a patient with sinus bradycardia and stress-induced bidirectional ventricular ectopy. The objectives of the present study were to determine if mice carrying the N98S mutation knocked into *Calm1* replicate the human arrhythmia phenotype and to examine arrhythmia mechanisms.

Methods: Mouse lines heterozygous for the $Calm1^{N98S}$ allele ($Calm1^{N98S/+}$) were generated using CRISPR/Cas9 technology. Adult mutant mice and their wildtype littermates ($Calm1^{+/+}$) underwent electrocardiographic monitoring. Ventricular de- and repolarization was assessed in isolated hearts using optical voltage mapping. Action potentials and whole-cell currents as well as $[Ca^{2+}]_i$ were measured in single ventricular myocytes using the patch-clamp technique and fluorescence microscopy, respectively. The microelectrode technique was employed for *in situ* membrane voltage monitoring of ventricular conduction fibers.

Results: Two biologically independent knock-in mouse lines heterozygous for the $Calm1^{N98S}$ allele were generated. $Calm1^{N98S/+}$ mice of either sex and line exhibited sinus bradycardia, QT_c

[#]**Address for correspondence:** (1) Michael Rubart, MD, Department of Pediatrics, Wells Center for Pediatric Research, Indiana University School of Medicine, 1044 West Walnut Street, Indianapolis, IN 46202 (mrubartv@iu.edu); phone: 317-407-1320; Fax: 317-278-9298; and (2) Peng-Sheng Chen, MD, current address: Department of Cardiology, Cedars-Sinai Medical Center, Los Angeles, CA, USA (ChenP3@cshs.org); Phone: 310-423-6084; Fax: 310-967-3891.

[*]These authors contributed equally to the manuscript.

Disclosures

None.

interval prolongation and catecholaminergic bidirectional ventricular tachycardia. Male mutant mice also showed QRS widening. Pharmacological blockade and activation of β-adrenergic receptors rescued and exacerbated, respectively, the long QT phenotype of Calm1$^{N98S/+}$ mice. Optical and electrical assessment of membrane potential in isolated hearts and single left ventricular myocytes, respectively, revealed β-adrenergically induced delay of repolarization. β-adrenergic stimulation increased peak density, slowed inactivation and left-shifted the activation curve of $I_{Ca.L}$ significantly more in Calm1$^{N98S/+}$ vs Calm1$^{+/+}$ ventricular myocytes, increasing late $I_{Ca.L}$ in the former. Rapidly paced Calm1$^{N98S/+}$ ventricular myocytes showed increased propensity to delayed afterdepolarization-induced triggered activity, whereas i*n situ* His-Purkinje fibers exhibited increased susceptibility for pause-dependent early afterdepolarizations. Epicardial mapping of Calm1$^{N98S/+}$ hearts showed that both reentry and focal mechanisms contribute to arrhythmogenesis.

Conclusions: Heterozygosity for the *Calm1*^{N98S} mutation is causative of an arrhythmia syndrome characterized by sinus bradycardia, QRS widening, adrenergically mediated QT_c interval prolongation and bidirectional ventricular tachycardia. β-adrenergically induced $I_{Ca.L}$ dysregulation contributes to the long QT phenotype. Pause-dependent early afterdepolarizations and tachycardia-induced delayed afterdepolarizations originating in the His-Purkinje network and ventricular myocytes, respectively, constitute potential sources of arrhythmia in Calm1$^{N98S/+}$ hearts.

Keywords

animal model; calcium channel; calmodulin; cardiac arrhythmia; congenital heart disease

Introduction

Mutations in the calmodulin (CaM)-encoding genes *CALM1*, *CALM2* and *CALM3* have been linked to ventricular arrhythmias manifesting with features of catecholaminergic polymorphic ventricular tachycardia (CPVT) and/or long QT syndrome.[1–7] All three CaM genes elaborate an identical, 148-amino acid, calcium binding protein. Calcium binding alters CaM interaction with target proteins, modifying their function. Nyegaard et al identified a *de novo* heterozygous missense mutation in exon 5 of the *CALM1* gene, resulting in substitution of asparagine at position 98 with serine (N98S, start methionine denoted residue 1).[8] The patient was a 4-year-old girl presenting with sinus bradycardia, stress-induced bidirectional ventricular ectopy, and sudden cardiac death.[8] A *de novo* N98S mutation of a different CaM gene (*CALM2*) was identified in an unrelated 5-year-old boy diagnosed with long QT syndrome,[1] indicating that an identical amino acid substitution in two distinct CaM genes can give rise to divergent clinical phenotypes. The N98S mutation has been investigated in different *in vitro* models that demonstrated that it increases single-channel open probability of the cardiac ryanodine receptor (RyR2),[9] attenuates L-type Ca^{2+} channel inactivation,[10] and reduces activation of small conductance, Ca^{2+}-activated potassium (SK) channels.[11] It has thus been inferred that arrhythmias develop as a consequence of Ca^{2+} cycling abnormalities (e.g., higher Ca^{2+} wave activity) and/or electrical disturbances (e.g., prolonged action potential duration).[5,9–12] However, experimental evidence which causally links this mutation to occurrence of arrhythmias is lacking.

Accordingly, the goals of the present study were (1) to develop a knock-in mouse model carrier of a N98S *Calm1* mutation that is the mouse equivalent of the human N98S *CALM1* mutation,[13] (2) to provide proof of the concept that this mutation is directly causative of the type of stress-induced ventricular arrhythmias seen in human patients, and (3) to investigate mechanisms contributing to the mutant phenotype.

Methods

A detailed description of the methods used including those for statistical analyses is provided in the Supplemental Data. The study was approved by the Institutional Biosafety Committee, Institutional Animal Care and Use Committee of the Indiana University and the Methodist Research Institute, Indianapolis, Indiana. All procedures were in accordance with the ethical standards of the responsible committees (institutional and national) on human experimentation.

Statistical analyses.

In all cases, data distribution was tested using Shapiro–Wilk's normality test. The 2-tailed, independent or paired sample *t*-test was used for comparison of normally distributed data. The 2-tailed independent sample Mann–Whitney's *U*-test was used for comparison of not-normally distributed data. One way Repeated Measures Analyses of Variance or Kruskal Wallis Mean Rank Sum test followed by appropriate post hoc analyses were used for comparisons of repeated measurements. Analyses of Covariance was used to test the effect of genotype on the linear dependence of ln QT on ln RR. A *P* value of less than or equal to 0.05 was considered significant. Values are presented as either mean ± SEM, or median with interquartile range. Experimenters were blinded to the genotype of the animals. SigmaPlot (Systat Software, Inc., San Jose, CA) was used for all statistical analyses.

Results

Generation of Calm1$^{N98S/+}$ mice

We used the CRISPR/Cas9 gene editing approach to generate knock in mice heterozygous for the N98S mutation in the *Calm1* gene (Calm1$^{N98S/+}$ mice; see Supplemental Data and Figure I in the Supplement for details). Two independent mouse lines were generated, designated line 2 and line 18. Calm1$^{N98S/+}$ mice were born at expected Mendelian ratios, exhibited normal growth, and survived to adulthood. Structure and contractile function of Calm1$^{N98S/+}$ hearts were normal (Table I and Figure II in the Supplement). There was no evidence for fibrosis. Relative quantification of *Calm1*, *Calm2* and *Calm3* transcripts in left ventricle of adult Calm1$^{+/+}$ and Calm1$^{N98S/+}$ mice by use of the $2^{-\Delta CT}$ method demonstrated that expression levels of each of the three *Calm* genes remained unchanged in Calm1$^{N98S/+}$ mice compared to their expression in littermate Calm1$^{+/+}$ mice (Table II in the Supplement), suggesting that the presence of a single N98S *Calm1* allele did not significantly alter transcription of any of the three *Calm* genes in mouse heart.

Phenotypic characterization

To evaluate the effects of the N98S *Calm1* mutation on cardiac electrical function *in vivo*, we examined the ECGs of conscious mice derived from continuous recordings via an implantable telemeter. Representative ECG examples are presented in Figure 1A, revealing sinus bradycardia, QT prolongation and QRS widening in the Calm1$^{N98S/+}$ mice. Twenty-four-hour plots of the mean RR, QT_c and QRS intervals were generated from long-term ECG recordings (see Supplemental Data and Figure III in the Supplement for a description of the method that was used to calculate QT_c intervals). As shown in Figure IV A in the Supplement, Calm1$^{N98S/+}$ mice exhibited increases in all three parameters for most of the 24-h period. Mean values of 24-h RR, QT_c and QRS intervals were significantly larger in Calm1$^{N98S/+}$ versus Calm1$^{+/+}$mice (Figure 1B) of either line. While the mean 24-h RR interval was significantly larger in line 18 vs line 2 Calm1$^{N98S/+}$ mice (left upper panel of Figure 1B), the differences for mean 24-h QT_c and QRS intervals between Calm1$^{+/+}$ and Calm1$^{N98S/+}$ mice were of similar magnitude (Figure 1B). Thus, Calm1$^{N98S/+}$ mice of two independently generated knock-in lines exhibited almost identical electrocardiographic phenotypes, characterized by sinus bradycardia, long QT and QRS widening.

Calm1$^{N98S/+}$ mice are susceptible to inducible ventricular arrhythmia

Treadmill exercise followed by epinephrine injection did not evoke arrhythmias (see Supplementary Data). Combined administration of caffeine and epinephrine has been used to elicit ventricular arrhythmias in different mouse models of CPVT.[14,15] Accordingly, we administered epinephrine (2 mg per kg body weight i.p.) and caffeine (120 mg per kg body weight i.p.) to 13 mice of line 2 (6 Calm1$^{+/+}$ and 7 Calm1$^{N98S/+}$) and 15 mice of line 18 (7 Calm1$^{+/+}$ and 8 Calm1$^{N98S/+}$) while continuously monitoring their ECG via telemetry. Representative ECGs recorded from Calm1$^{+/+}$ and Calm1$^{N98S/+}$ littermates (line 2) before and following a single caffeine and epinephrine injection are shown in Figure 1C. The Calm1$^{+/+}$ mouse developed transient sinus tachycardia, but ventricular tachyarrhythmias were not observed during the 30-min period of post injection telemetric ECG recording. Overall, 6 out of 7 line 2 Calm1$^{+/+}$ mice receiving epinephrine and caffeine did not have ventricular tachyarrhythmias within the 30-min post injection intervals, while one Calm1$^{+/+}$ mouse exhibited repetitive episodes of ventricular bigeminy (duration ranging from 5 s to 324 s) post injection. In contrast, administration of epinephrine and caffeine to the Calm1$^{N98S/+}$ mouse triggered ventricular bigeminy which was followed by a 25-s episode of tachycardia displaying beat-to-beat alternations in the polarity of the QRS axis as well as atrio-ventricular dissociation (Figure 1C and D), consistent with bidirectional ventricular tachycardia (BVT), a hallmark of CPVT.[15] In one Calm1$^{N98S/+}$ mouse, BVT transitioned into polymorphic VT (Figure 1E). Overall, 7 out of 7 Calm1$^{N98S/+}$ mice of line 2 exhibited at least one episode of pharmacologically induced, sustained BVT, indicating high penetrance ($P < 0.001$ versus Calm1$^{+/+}$; Figure 1F). All VT episodes reverted spontaneously to sinus rhythm. Identical results for arrhythmia inducibility were obtained in mice of line 18 (Figure 1F). Cumulative incidence, cycle length, and coupling interval ratio (see Figure IV B in the Supplement) of induced BVT episodes were indistinguishable between Calm1$^{N98S/+}$ mice of the two lines, whereas their cumulative duration was significantly longer in line 18 mutants (Figure 1G). Finally, the cumulative incidence of premature ventricular contractions (PVCs) per 24 h as well as the 24-h arrhythmia scores were significantly elevated in

Calm1$^{N98S/+}$ versus Calm1$^{+/+}$ mice of either mouse line, but their respective mean values were similar between genotypically identical mice in the two lines (Figure IV C in the Supplement).

We also compared the electrical phenotype between conscious female and male mice of line 2. The results are summarized in Figure V in the Supplement. Like their male counterparts, female Calm1$^{N98S/+}$ mice exhibited sinus bradycardia and QT_c interval prolongation, but QRS duration was not prolonged in female Calm1$^{N98S/+}$ mice (Figure V A and B in the Supplement). Mean 24-h QT_c intervals in female Calm1$^{+/+}$ and Calm1$^{N98S/+}$ mice were significantly shorter than those in their male counterparts (Figure V B in the Supplement). Co-administration of epinephrine and caffeine induced sustained BVT in 7 out of 8 female and 7 out of 7 male Calm1$^{N98S/+}$ mice, but in none of the Calm1$^{+/+}$ males or females (Figure V C and D in the Supplement). Median incidence of BVT was significantly lower in female than male Calm1$^{N98S/+}$ mice, whereas mean values for cumulative duration, cycle length and coupling interval of BVT episodes were similar among male and female Calm1$^{N98S/+}$ mice of line 2 (Figure V E in the Supplement). The 24-h arrhythmia scores were not significantly different between Calm1$^{+/+}$ males and females or between Calm1$^{N98S/+}$ males and females. Together, these results indicate that the arrhythmia phenotype presents with extraordinary similarity between Calm1$^{N98S/+}$ mice from two independently generated knock-in lines, irrespective of sex. Accordingly, all following experiments utilized male mice from one line only (line 2).

β-adrenergic stimulation induces long QT phenotype in Calm1$^{N98S/+}$ mice

Modest increases in the QT_c and QRS intervals were found in Calm1$^{N98S/+}$ mice (Figure 1), compatible with abnormalities in both ventricular repolarization and conduction. To quantify the extent to which heterozygosity for the *Calm1*^{N98S} allele alters these electrophysiological parameters, we next performed epicardial optical voltage mapping of the anterior surface of 11 Langendorff-perfused Calm1$^{N98S/+}$ and 11 Calm1$^{+/+}$ hearts. Representative color activation maps during right atrial pacing at a cycle length of 120 ms are presented in Figure 2A. In both genotypes, activation pattern is characterized by 2 epicardial breakthroughs that originate on the free walls of the right and left ventricles near the apex (asterisks). These breakthroughs occur simultaneously and form wave fronts that propagate towards the bases of the hearts, fully activating the field of view within 6 ms and 8 ms in the Calm1$^{+/+}$ and Calm1$^{N98S/+}$ hearts, respectively. To determine whether conduction defects within the ventricular myocardium contribute to QRS widening in the Calm1$^{N98S/+}$ mice, epicardial conduction patterns and velocities were determined. Figure 2B shows activation maps obtained from the anterior aspect of a Calm1$^{+/+}$ and a Calm1$^{N98S/+}$ heart while pacing the ventricles directly at a cycle length of 100 ms. The anisotropic conduction pattern in the Calm1$^{N98S/+}$ heart was similar to that of Calm1$^{+/+}$. Figure 2C shows dot plots of CV_{max} and CV_{min} for all Calm1$^{+/+}$ and Calm1$^{N98S/+}$ hearts tested. No statistically significant differences were found between the two genotypes. These data indicate that the QRS widening seen in Calm1$^{N98S/+}$ mice is unlikely to result from conduction disturbances in the ventricular myocardium.

Exemplar color repolarization maps obtained from atrial paced hearts (120 ms cycle length) of either genotype are shown in Figure 2D. Ventricular action potential durations (APD) at 30%, 50% and 80% repolarization were longer in the $Calm1^{N98S/+}$ versus $Calm1^{+/+}$ heart. The mean values for APD_{30}, APD_{50} and APD_{80} were modestly, yet significantly, larger in $Calm1^{N98S/+}$ hearts (Figure 2E), in agreement with the modest QT_c prolongation observed in $Calm1^{N98S/+}$ mice *in vivo*. These results support the notion that abnormal ventricular repolarization underlies the long QT phenotype of $Calm1^{N98S/+}$ mice. While combined exposure of isolated hearts of either genotype to epinephrine (1.6 μmol/L) and caffeine (5 mmol/L) failed to induce ventricular arrhythmias, it reversibly prolonged APD_{80} significantly more in $Calm1^{N98S/+}$ versus $Calm1^{+/+}$ hearts as shown in Figure 2F and G. Treatment of two Langendorff-perfused $Calm1^{N98S/+}$ hearts with the non-selective β-adrenergic receptor agonist isoproterenol (100 nM) quantitatively replicated the increases in APD_{80} seen in the presence of epinephrine and caffeine (Figure VI in the Supplement), while it did not significantly affect ventricular activation patterns or conduction velocities (not shown). These data indicate that activation of cardiac β-adrenergic receptors mediates excessive APD prolongation in $Calm1^{N98S/+}$ hearts treated with epinephrine/caffeine.

We next recorded action potentials from single ventricular myocytes under current clamp. Exemplar recordings obtained at 1 and 7 Hz pacing rates show similar action potential shape and time course in $Calm1^{+/+}$ and $Calm1^{N98S/+}$ myocytes (Figure 3A). Figure 3B shows dot plots for APD_{30}, APD_{50} and APD_{90} for all cells tested. No statistically significant differences were found between the 2 genotypes. We also observed no differences in the resting membrane potential, action potential peak, or action potential upstroke velocity (Table III in the Supplement). These data raise the possibility that cardiomyocyte non-autonomous factors are responsible for the long QT phenotype of $Calm1^{N98S/+}$ mice. The optical mapping data obtained from $Calm1^{N98S/+}$ hearts suggested a critical role of altered responsiveness of the ventricular action potential to β-adrenergic receptor stimulation in mediating QT_c interval prolongation. Accordingly, we next compared isoproterenol (50 nmol/L)-induced changes in action potential properties of $Calm1^{N98S/+}$ ventricular myocytes with myocytes from $Calm1^{+/+}$ littermates. Representative action potential traces are presented in Figure 3C. While isoproterenol had no significant effect on the action potential repolarization in $Calm1^{+/+}$ myocytes, it markedly and reversibly delayed late repolarization (APD_{90}; Figure 3D) in $Calm1^{N98S/+}$ myocytes. Isoproterenol did not significantly change early repolarization (APD_{30} and APD_{50}), resting membrane potential, action potential peak or maximal upstroke velocity in cells of either genotype (Table IV in the Supplement). Isoproterenol-induced, excessive APD prolongation impeded 1:1 stimulus-action potential responses in the majority of isolated $Calm1^{N98S/+}$ myocytes at 7 Hz pacing, preventing reliable APD measurements. We did not observe early afterdepolarizations in control or isoproterenol-treated myocytes of either genotype. In control conditions, none of 13 $Calm1^{+/+}$ and 14 $Calm1^{N98S/+}$ ventricular myocytes (distributed among 3 $Calm1^{+/+}$ and 4 $Calm1^{N98S/+}$ mice, respectively) developed delayed afterdepolarizations (DAD) at 1 Hz pacing, whereas one myocyte of either genotype generated one DAD each at 7 Hz pacing ($P = 1.0$ by *Fisher Exact* test). The fraction of isoproterenol-treated $Calm1^{N98S/+}$ myocytes exhibiting DAD-triggered action potentials at 7 Hz pacing (8 out of 10 cells distributed among 2 mice; Figure 3E) was significantly higher than that of isoproterenol-treated

Calm1$^{+/+}$ myocytes (1 out of 7 cells; 2 mice; $P = 0.015$ by *Fisher Exact* test), whereas no significant differences were found between isoproterenol-treated myocytes of the 2 genotypes during 1 Hz pacing (1 out of 7 Calm1$^{+/+}$ myocytes versus 0 out of 10 Calm1$^{N98S/+}$ myocytes; $P = 0.412$ by *Fisher Exact* test).

Finally, we assessed the effects of pharmacological β-adrenergic receptor inhibition and activation on heart rate and durations of QRS and QT_c intervals in conscious mice implanted with wireless ECG transmitters. Administration of propranolol (a non-selective β-adrenergic receptor blocker; 1 mg/kg i.p.) or isoproterenol (0.17 mg/kg i.p.) significantly reduced and increased, respectively, mean heart rate in mice of either genotype, but significant heart rate differences between genotypes persisted in the presence of either drug (Figure 3F). Propranolol rescued the QT_c interval prolongation of Calm1$^{N98S/+}$ mice, while isoproterenol aggravated the relatively modest baseline differences in QT_c interval between Calm1$^{+/+}$ and Calm1$^{N98S/+}$ mice (Figure 3G and H). Neither drug significantly affected QT_c interval in Calm1$^{+/+}$ mice and QRS duration in either genotype (not shown). No ventricular tachycardias were observed in either genotype. Taken together, the *in vitro* and *in vivo* data indicate that manifestation of the long QT phenotype of Calm1$^{N98S/+}$ mice requires stimulation of cardiac β-adrenergic receptors.

Epicardial voltage mapping of ventricular arrhythmias

Our current-clamp measurements revealed delayed afterdepolarization-mediated triggered activity in rapidly paced Calm1$^{N98S/+}$ ventricular cardiomyocytes in the presence of isoproterenol suggesting involvement of focal mechanisms in the genesis of catecholaminergic arrhythmias in the mutant mice. The concomitant, isoproterenol-induced APD prolongation, if occurring in a spatially and/or temporally discordant manner, could also facilitate reentrant activity. We used epicardial optical voltage mapping of isolated perfused Calm1$^{+/+}$ and Calm1$^{N98S/+}$ hearts to investigate arrhythmia mechanisms associated with elevated extracellular calcium and/or catecholaminergic stimuli. Exposure to epinephrine and caffeine did not evoke ventricular arrhythmias in atrial paced (120 ms cycle length), blebbistatin-treated Calm1$^{N98S/+}$ (n=6) or Calm1$^{+/+}$ hearts (n=8). Other isolated, non-paced hearts were perfused with blebbistatin-free Tyrode's solution containing 3.6 mmol/L $CaCl_2$ plus 100 nmol/L isoproterenol (4 hearts per genotype) and subjected to programmed electrical stimulation and burst stimulation. None of the Calm1$^{+/+}$ hearts showed spontaneous or inducible arrhythmias. In contrast, one Calm1$^{N98S/+}$ heart each had spontaneous or burst-induced episodes of VT as shown in Figure 4 and Figure VII in the Supplement, respectively. Each VT episode in Figure 4 is triggered by a ventricular ectopic beat, sharing the same morphology as the single ectopic beat (complex 2), suggesting a common focal origin. Indeed, voltage maps of the VT episodes revealed focal discharges on the right ventricular free wall which coincided with the emergence of the triggering ectopic beats on the ECG, as shown exemplarily for the first NSVT episode. Their concentric breakthrough patterns were similar to those emanating from the right ventricular free wall during sinus rhythm (Figure 4A). The RV focal discharges initiated NSVT for 2–4 cycles. The last QRS complexes of each episode were associated with the emergence of an RV (complex 6) or LV focal discharge, exhibiting breakthrough patterns similar to those seen during sinus rhythm. Figure VII in the Supplement shows an episode of a non-sustained VT

following a 1-s train of stimuli at 100 Hz in another Calm1$^{N98S/+}$ heart. This VT episode also exhibited a combined mechanism of right ventricular focal trigger and macro-reentry. BVT was not observed in either one of the 2 Calm1$^{N98S/+}$ hearts. In addition, non-paced Calm1$^{N98S/+}$ hearts perfused with 200 nmol/L isoproterenol and elevated Ca^{2+} (n=4), 1.6 μmol/L epinephrine, 5 mmol/L caffeine and elevated Ca^{2+} (n=2), or 1.6 μmol/L epinephrine plus 5 mmol/L caffeine (n = 1), but not undergoing programmed or burst stimulation, showed no arrhythmias. Taken together, these observations suggest that focal discharges initiated reentry in catecholaminergic arrhythmias of Calm1$^{N98S/+}$ mice.

Enhanced L-type Ca^{2+} current contributes to β-adrenergic stimulation-induced prolongation of action potential repolarization in Calm1$^{N98S/+}$ mice

A previous study has demonstrated that overexpression of N98S CaM in guinea-pig ventricular myocytes diminishes Ca^{2+}/CaM-dependent inactivation (CDI) of L-type Ca^{2+} channels,[10] suggesting that impaired L-type current inactivation contributes to the long QT phenotype of Calm1$^{N98S/+}$ mice. Accordingly, we next sought to examine the properties of whole-cell L-type Ca^{2+} currents, $I_{Ca.L}$, in single ventricular myocytes isolated from Calm1$^{+/+}$ and Calm1$^{N98S/+}$ mice. Measurements were performed under whole-cell voltage clamp with high intracellular Ca^{2+} buffering by 10 mM BAPTA and in the presence of ryanodine (5 μM) in the pipette solution, to restrict CDI to that driven by Ca^{2+} entering through individual L-type Ca^{2+} channels.[10] These measurements revealed attenuation of CDI and faster $I_{Ca.L}$ recovery from inactivation in Calm1$^{N98S/+}$ cardiomyocytes, but no significant differences for peak $I_{Ca.L}$ density or voltage-dependence of steady state activation and inactivation between the 2 genotypes (see Supplementary Data, Figure VIII and Table V in the Supplement).

Impaired CDI of L-type channels in combination with their accelerated recovery from inactivation in Calm1$^{N98S/+}$ ventricular myocytes would be expected to enhance L-type Ca^{2+} current during the action potential, delaying its repolarization. Since we did not, however, observe significant prolongation of action potential duration in isolated Calm1$^{N98S/+}$ ventricular myocytes under baseline conditions, the magnitude of changes in L-type channel gating was either insufficient to significantly lengthen action potentials or experimental conditions used for action potential recording blunted N98S CaM-mediated alterations of L-type channel gating. Measurements of macroscopic L-type currents were obtained with high intracellular Ca^{2+} buffering in the presence of ryanodine, while action potentials were recorded under more physiological Ca^{2+} buffering (0.5 mM EGTA), allowing global elevations of Ca^{2+}. Accordingly, we next obtained the equivalent whole-cell patch-clamp data using a ryanodine-free pipette solution containing 1 mM EGTA. Results are summarized in Figure 5, Figure IX in the Supplement and Table VI in the Supplement. We observed no significant differences in the peak $I_{Ca.L}$ density-voltage relations (Figure 5A and B), voltage-dependence of steady-state activation and inactivation (Figure 5E), time course of $I_{Ca.L}$ inactivation (Figure 5G, H), and recovery from inactivation (Figure IX A and B in the Supplement) between the two genotypes under baseline conditions. In sharp contrast, isoproterenol (50 nM) increased peak $I_{Ca.L}$ density (Figure 5C and D), left-shifted the steady-state activation curve (Figure 5F), increased the non-inactivating pedestal of the inactivation curve (Figure 5F), and slowed $I_{Ca.L}$ inactivation (Figure 5G and H) significantly

more in Calm1$^{N98S/+}$ versus Calm1$^{+/+}$ myocytes (Table VI in the Supplement). Isoproterenol also modestly reduced maximal $I_{Ca.L}$ recovery from inactivation but did not significantly affect the recovery time constant (Figure IX C,D and Table VI in the Supplement). A more pronounced left shift of the steady-state activation curve combined with augmentation of peak $I_{Ca.L}$ is expected to significantly increase the *L*-type window or late current (late $I_{Ca.L}$) within a voltage range that extends from threshold to potentials above the V_{peak} of the *I-V* relation (inset Figure 5F). Accordingly, we next measured total L-type Ca^{2+} current under action potential – clamp conditions both in the presence and absence of 50 nM isoproterenol. L-type Ca^{2+} currents were elicited by 'typical' action potential waveforms that had been pre-recorded from control and isoproterenol-treated Calm1$^{+/+}$ and Calm1$^{N98S/+}$ ventricular myocytes during steady-state pacing at 1 Hz. Results are summarized in Figure 6 and Figure X in the Supplement. Switching between action potentials pre-recorded in control Calm1$^{+/+}$ and Calm1$^{N98S/+}$ myocytes did not significantly change mean amplitudes of peak $I_{Ca.L}$ or total $I_{Ca.L}$ ($\int I_{Ca.L}$) in myocytes of either genotype in the absence of isoproterenol (Figure X in the Supplement). In its presence, however, magnitudes of both mean peak $I_{Ca.L}$ and mean $\int I_{Ca.L}$ using the waveforms obtained from isoproterenol-treated myocytes of either genotype were significantly smaller in Calm1$^{+/+}$ myocytes than the ones that resulted when the same waveforms were imposed on Calm1$^{N98S/+}$ myocytes (Figure 6). Expanded views of the action potential waveforms and $I_{Ca.L}$ traces (Figure 6C and D) demonstrate that $I_{Ca.L}$ remains elevated throughout action potential repolarization in isoproterenol-treated Calm1$^{N98S/+}$ versus Calm1$^{+/+}$ myocytes. Taken together these results indicate that heterozygosity for the *Calm1^{N98S}* allele potentiates β-adrenergic effects on *L*-type channel gating, leading to increases in both peak and late $I_{Ca.L}$ during the ventricular action potential.

Both Ca^{2+}-free and Ca^{2+}-bound calmodulin modulate properties of cardiac voltage-gated Na^+ channels via direct or indirect (through Ca^{2+}/CaM kinase II) interactions.[16] We found no differences for peak I_{Na} density, steady-state activation or inactivation, recovery from inactivation, or inactivation kinetics between Calm1$^{+/+}$ and Calm1$^{N98S/+}$ ventricular myocytes (Figure XI A–E and Table VII in the Supplement), in agreement with a lack of a significant difference for ventricular conduction velocity between hearts of the 2 genotypes (Figure 2B and C). We also found no significant differences between the two genotypes for late Na^+ current in the absence or presence of isoproterenol (Figure XI F and G in the Supplement). These findings support the idea that L-type Ca^{2+}, but not Na^+, channel dysregulation contributes to β-adrenergic receptor stimulation-induced prolongation of ventricular action potential repolarization and thus appears to be critical for manifestation of the long QT phenotype of Calm1$^{N98S/+}$ mice.

Cardiomyocyte Ca^{2+} cycling

Previous *in vitro* evidence led to the hypothesis that heightened propensity of ventricular myocytes for abnormal diastolic Ca^{2+} release events resulting from RyR2 disinhibition contributes to catecholamine-induced arrhythmias associated with the N98S CaM mutation.[9] To examine RyR2 function, we next analyzed Ca^{2+} sparks in single, intact ventricular myocytes.[17] Figure 7A and B shows that resting spark frequency in the absence of isoproterenol was decreased by ca. 50% in Calm1$^{N98S/+}$ myocytes, indicating reduced RyR2

channel activity, but rose to similar levels in both genotypes following isoproterenol exposure. Ca^{2+} spark amplitude (peak F/F_0; Figure 7C) was indistinguishable at baseline in cells of either genotype but significantly increased in $Calm1^{+/+}$, but not $Calm1^{N98S/+}$, myocytes following isoproterenol (1 μmol/L) treatment. We observed no significant isoproterenol effect on the spatial spread (FWHM) of Ca^{2+} sparks in myocytes of either genotype (Figure 7D). The spark duration (FDHM; Figure 7E) was longer in $Calm1^{N98S/+}$ myocytes both without and with isoproterenol, and the duration of the rising phase (time to peak) was significantly prolonged in $Calm1^{N98S/+}$ myocytes in the presence of isoproterenol (Figure 7F), compatible with an increase in the number of RyR2 channels recruited during a spark and/or delayed termination of SR Ca^{2+} release flux. The changes in Ca^{2+} spark properties may promote the development of spontaneous Ca^{2+} aftertransients. Accordingly, we next assessed the response of action potential-evoked whole-cell $[Ca^{2+}]_i$ transients to isoproterenol. Isoproterenol (1 μmol/L) similarly increased steady-state twitch $[Ca^{2+}]_i$ amplitude in the 2 genotypes and caused plateau-like $[Ca^{2+}]_i$ elevations lasting ~100 ms in $Calm1^{N98S/+}$ myocytes, delaying return of $[Ca^{2+}]_i$ to baseline (Figure XII in the Supplement). We found no evidence for increased propensity of $Calm1^{N98S/+}$ ventricular myocytes to develop early or delayed Ca^{2+} aftertransients under baseline conditions or during isoproterenol (1 μmol/L) treatment at pacing frequencies ranging from 1 to 3 Hz (Figure XIII in the Supplement).

Increased propensity of the His-Purkinje system of $Calm1^{N98S/+}$ hearts for pause-dependent early afterdepolarizations

BVT has been previously suggested to originate from afterdepolarization-induced triggered activity generated in the His-Purkinje network.[18,19] To examine whether the His-Purkinje system of $Calm1^{N98S/+}$ hearts is susceptible to the development of pro-arrhythmic afterdepolarizations, electrical recordings were obtained from the right bundle branch as well as from the web and the septal endocardium in the right ventricles at baseline, during treatment with 100 nM isoproterenol, and following washout. Representative action potentials are shown in Supplemental Figure 14A and action potential parameters are summarized in Supplemental Table 8. Baseline APD_{90} was significantly longer in $Calm1^{N98S/+}$ versus $Calm1^{+/+}$ conduction fibers. Isoproterenol prolonged APD_{30}, APD_{50} and APD_{90} in myocytes of either genotype, while significant differences for APD_{90} remained (Figure XIV B and C in the Supplement). Interruption of steady-state pacing resulted in the development of pause-dependent phase 2 or phase 3 early afterdepolarizations (EADs; Figure 8A and B) in 34 of 67 $Calm1^{N98S/+}$ conduction fibers, but in only 6 of 55 $Calm1^{+/+}$ fibers ($P < 0.001$ by *Chi-square* test; Figure 8C). Isoproterenol did not significantly alter the incidence of EADs compared to baseline in cells of either genotype. Take-off potentials of a total of 202 and 23 EADs in $Calm1^{N98S/+}$ and $Calm1^{+/+}$ fibers, respectively, ranged from −75 mV to −29 mV and from −65 mV to −43 mV. Mean values for take-off potential and amplitude of EADs were similar between the 2 genotypes, whereas the mean diastolic interval preceding EAD-containing action potentials was shorter in $Calm1^{+/+}$ cells (Figure 8C). Delayed afterdepolarizations were never observed in wedges from either genotype. Taken together, these findings demonstrate that heterozygosity for the $Calm1^{N98S}$ allele predisposes right ventricular conduction fibers to the development of pause-dependent EADs. Activation of β-adrenergic receptors did not promote EAD formation.

Discussion

This study provides, to the best of our knowledge, the first proof that the presence of N98S CaM is able to induce sustained ventricular arrhythmias on exposure to caffeine and epinephrine. Specifically, the arrhythmia phenotype of the murine model that we developed presents remarkable similarity with the clinical manifestation of the patient carrier of the N98S mutation in terms of arrhythmia morphology and inducibility by stress.[8] Furthermore, Calm1$^{N98S/+}$ mice exhibited sinus bradycardia which was also present in the human patient. Besides these phenotypic commonalities, QT_c interval prolongation was not reported for the human carrier of the N98S *CALM1* mutation. Manifestation of the long QT phenotype in Calm1$^{N98S/+}$ mice requires stimulation of β-adrenergic receptors. Because plasma norepinephrine levels in mice are typically more than an order of magnitude above values reported for humans,[20,21] enhanced basal sympathetic tone in the Calm1$^{N98S/+}$ mice may have contributed to the discrepancies between the human and murine phenotype.

Although the CRISPR/Cas9-mediated knock-in procedure may cause off-target mutagenesis which can confound interpretation of the genotype-phenotype relationship,[22] we do not believe this is the case here. Calm1$^{N98S/+}$ mice generated from two independent integration events were essentially phenotypically identical. In addition, animals were analyzed after multiple back cross generations into a new inbred background, thus greatly diluting any contribution of an off-target event in the original targeted genome. Thus, contributions of off-target sites to the phenotypes observed in our mice are unlikely, strengthening our conclusion that heterozygosity for the Calm1^{N98S} allele is causative of the arrhythmia syndrome. We further found no evidence that the cardiac phenotype developed secondary to cardiac structural abnormalities or contractile dysfunction.

Mechanisms of QT prolongation

Our data indicates a key role of β-adrenergic induced $I_{Ca.L}$ dysregulation in the pathogenesis of the long QT phenotype of Calm1$^{N98S/+}$ mice. β-adrenergic receptors signal through the G_s protein-adenylyl cyclase-cAMP-PKA pathway to regulate *L*-type channels.[23] Functionally, β-adrenergic receptor stimulation elevates the activity of L-type channels as a result of an increase in the channel's open probability.[24] As a consequence, macroscopic $I_{Ca.L}$ amplitude increases, voltage-dependence of steady-state activation shifts to more negative potentials, and the inactivation rates accelerate. We observed that isoproterenol both increased peak $I_{Ca.L}$ and left-shifted the activation curve significantly more in Calm1$^{N98S/+}$ versus Calm1$^{+/+}$ ventricular cardiomyocytes (Figure 5), supporting the notion that N98S CaM potentiated β-adrenergic effects on *L*-type channel gating, increasing the magnitude of window $I_{Ca.L}$ in mutant cardiomyocytes. Inactivation rates remained diminished in isoproterenol-treated Calm1$^{N98S/+}$ myocytes (Figure 5H). Taken together, these findings suggest a mechanism wherein attenuation of $I_{Ca.L}$ inactivation pairs with β-adrenergic enhancement of window $I_{Ca.L}$ to give rise to elevated 'late' $I_{Ca.L}$ in Calm1$^{N98S/+}$ ventricular myocytes, prolonging their action potential duration. A role of adrenergic – induced *L*-type channel dysregulation in delaying ventricular repolarization is directly supported by our action potential-clamp data, showing augmented Ca^{2+} influx extending throughout action potential repolarization of isoproterenol-treated Calm1$^{N98S/+}$ myocytes. Overall, our data is

compatible with the concept that N98S CaM-dependent attenuation of $I_{Ca.L}$ inactivation in concert with potentiation of β-adrenergic-mediated effects on L-type Ca^{2+} channels is responsible, at least in part, for the adrenergic induced long QT phenotype of $Calm1^{N98S/+}$ mice.

L-type channels and small-conductance, Ca^{2+}-gated K^+ (SK) channels form a negative feedback system wherein Ca^{2+} influx through *L*-type Ca^{2+} channels directly activates SK channels, preventing excessive repolarization prolongation.[25] We have previously demonstrated that N98S CaM impedes activation of heterologously expressed SK channels, [11] raising the possibility that inadequate SK channel activation contributes to manifestation of the long QT phenotype of $Calm1^{N98S/+}$ mice.

Both Ca^{2+}-free and Ca^{2+}-bound calmodulin, via direct and indirect interactions, regulate gating of cardiac, voltage-activated Na channels. Specifically, calmodulin has been shown to control the magnitude of late I_{Na}, an important determinant of ventricular action potential duration.[16,26] β-adrenergic receptor stimulation also enhances late I_{Na}.[27] However, we found no evidence for a role of elevated late I_{Na} in prolonging ventricular repolarization in control or isoproterenol-treated $Calm1^{N98S/+}$ ventricular cardiomyocytes.

Calmodulin also regulates gating of voltage-activated K^+ channels, via direct interaction or indirectly via Ca^{2+}/CaMKII.[28] We did not, however, observe significant differences in the time course of early repolarization nor in resting membrane potential between isoproterenol-treated $Calm1^{+/+}$ and $Calm1^{N98S/+}$ ventricular cardiomyocytes, suggesting that activities of transient outward K^+ currents and inward rectifier K^+ currents, respectively, remained largely unaffected. Although calmodulin has been shown to regulate delayed rectifier K^+ currents (I_{Ks}),[29] ventricular cardiomyocytes of adult mice do not elaborate significant I_{Ks}, excluding I_{Ks} as a long QT-causing candidate in our model.

Female mice of either genotype had significantly shorter QT_c intervals compared to genotype-matched males. Previous reports revealed that QT_c intervals of adult female mice are shorter than those of age-matched males during stages of the estrous cycle when estrogen levels are low (which occurs typically for 3.5 days of the 4-day cycle).[30] Although we did not ascertain the estral stage during telemetry, the significantly shorter QT_c intervals seen in female mice suggest that they were under low-estrogen conditions during ECG monitoring. Their shorter QT_c intervals, however, did not protect female $Calm1^{N98S/+}$ mice from inducible arrhythmias.

Arrhythmogenic mechanisms

Our microelectrode studies revealed a markedly increased propensity of the right ventricular His-Purkinje network of $Calm1^{N98S/+}$ hearts to generate pause-dependent early, but not delayed, afterdepolarizations. Isoproterenol did not augment the incidence of early afterdepolarizations, suggesting that β-adrenergic activation promotes their transmission to the surrounding myocardium rather than their formation in the conduction system. Voltage mapping revealed a right ventricular focal origin of the VT-triggering ectopic beats in $Calm1^{N98S/+}$ hearts perfused with elevated Ca^{2+} and isoproterenol. Intriguingly, these ectopic beats manifested as concentric epicardial breakthrough patterns that were similar to

those emanating from the right ventricular free wall during normal sinus rhythm, suggesting a focal origin in the His-Purkinje network. Thus, our findings support the possibility that focal discharges arising from early afterdepolarization-induced triggered events within the ventricular conduction system contribute to catecholaminergic arrhythmogenicity in Calm1$^{N98S/+}$ hearts. However, whether BVT in our model is mediated by early afterdepolarization-induced triggered activity originating in Purkinje fibers needs to be determined. EAD take-off potentials were observed to occur over a range of membrane potentials wherein I_{CaL} reactivation is limited, suggesting other ionic mechanisms also contribute to EAD formation, possibly including Na/Ca exchanger current and/or I_{Na}.[31]

DAD-induced triggered responses occurred in isoproterenol-treated Calm1$^{N98S/+}$ ventricular myocytes at high pacing rates, suggesting their involvement in arrhythmogenesis. Transition from BVT into PVT as observed in one Calm1$^{N98S/+}$ mouse after combined epinephrine and caffeine administration may be attributed to focal discharges mediated by DADs arising at multiple locations within the working myocardium. Thus, EADs in the His-Purkinje network and DADs in the working myocardium may serve complementary roles in initiating and maintaining, respectively, arrhythmias in our model. The similarly low prevalence of delayed Ca^{2+} aftertransients in isoproterenol-challenged ventricular myocytes of both genotypes is at odds with the increased susceptibility of Calm1$^{N98S/+}$ myocytes to the development of DAD-induced triggered responses at high pacing rates. We cannot readily explain this discrepancy. It is possible that the higher maximum pacing rate used in the current-clamp (7 Hz) versus imaging (3 Hz) experiments is critical to detect genotype-specific differences in the susceptibility to DAD-causing, spontaneous SR calcium release events. For example, a higher integrated Ca^{2+} influx through adrenergically activated *L*-type channels during rapid pacing may lead to a larger SR Ca^{2+} load of Calm1$^{N98S/+}$ myocytes, promoting RyR2 opening. However, the contribution of SR Ca^{2+} load versus that of other mechanisms (N98S CaM-mediated RyR2 disinhibition[9], differences in cytosolic [Ca^{2+}]) to arrhythmogenic Ca^{2+} release events remains to be determined.

Role of bradycardia in catecholaminergic BVT

Like the human carrier of the N98S *CALM1* mutation, Calm1$^{N98S/+}$ mice exhibited chronic sinus bradycardia. Sinus node rates increased in mice of either genotype in response to β-adrenergic receptor stimulation but remained lower in Calm1$^{N98S/+}$ than in Calm1$^{+/+}$ mice. Such chronotropic incompetence paired with adrenergic induced QT_c interval prolongation may promote EAD-induced triggered discharges in the ventricular conduction system.

The persistence of sinus bradycardia following pharmacological blockade and activation of β-adrenergic receptors in Calm1$^{N98S/+}$ mice suggested a change in the intrinsic firing rate of sinus node myocytes through modulation of proteins involved in pacemaking (e.g., ryanodine receptor, Na^+/Ca^{2+} exchanger),[32,33] either directly via binding to them or indirectly via changes in Ca^{2+}/CaMKII activity.[33,34] Impulse transmission from the sinus node cells to the atrial myocardium is mediated by different voltage-gated sodium channel isoforms[35] which are regulated by CaM[36] as well as Ca^{2+}/CaMKII and can thus be impaired following N98S-CaM binding.

QRS widening

QRS widening, indicative of ventricular conduction slowing, was seen in conscious male Calm1$^{N98S/+}$ mice but was not reported for the human female carrier. Using optical voltage mapping of Langendorff-perfused hearts, we found no evidence for ventricular conduction slowing in control or isoproterenol-treated Calm1$^{N98S/+}$ hearts, in agreement with the similar properties of voltage-gated fast Na^+ current in ventricular cardiomyocytes of the two genotypes. We also observed no statistical differences for action potential amplitude or maximal phase 0 upstroke velocity between Calm1$^{N98S/+}$ and Calm1$^{+/+}$ His-Purkinje myocytes *in situ*, neither in control nor during β-adrenergic stimulation, suggesting that impulse propagation within the ventricular conduction system of *ex vivo* Calm1$^{N98S/+}$ hearts was intact. Thus, we cannot readily explain the mechanism underlying QRS complex widening in male Calm1$^{N98S/+}$ mice. A potential role of autonomic innervation in decelerating conduction in the *in situ* Calm1$^{N98S/+}$ heart that may be absent or attenuated in the isolated heart cannot be discarded.

Conclusions

Our data provide proof of the concept that heterozygosity for the *Calm1*^{N98S} mutation is causative of a complex arrhythmia syndrome characterized by sinus bradycardia, adrenergically induced QT_c interval prolongation, and susceptibility to the development of catecholaminergic BVT. Heterozygosity for the Calm1^{N98S} allele attenuates Ca^{2+}/CaM-dependent $I_{Ca.L}$ inactivation and potentiates β-adrenergic effects on cardiac *L*-type Ca^{2+} current, leading to elevated late $I_{Ca.L}$ which prolongs ventricular repolarization. Pause-dependent EADs and rapid pacing-induced DADs originating in the His-Purkinje network and ventricular myocytes, respectively, constitute a potential source of catecholaminergic BVT.

Supplementary Material

Refer to Web version on PubMed Central for supplementary material.

Acknowledgments

Sources of Funding

The work was supported by an American Heart Association Postdoctoral Fellowship (W.C.T), the 2013 International Fellowship Training Program (Basic research) from the Asia-Pacific Heart Rhythm Society (W.C.T.), the National Institutes of Health (P01 HL78931, R42DA043391, R01 HL139829 and OT2OD028190; P.S.C.), a Medtronic-Zipes Endowment, and the Indiana University Health-Indiana University School of Medicine Strategic Research Initiative.

Non-standard Abbreviations and Acronyms

APD	action potential duration
BVT	bidirectional ventricular tachycardia
CaM	calmodulin
CDI	Ca^{2+}/CaM-dependent inactivation

CPVT	catecholaminergic polymorphic ventricular tachycardia
CV	conduction velocity
DAD	delayed afterdepolarization
EAD	early afterdepolarization
FDHM	full duration at half maximum
FWHM	full width at half maximum
PVT	polymorphic ventricular tachycardia
QT_c	corrected QT interval
RyR2	ryanodine receptor type 2
SK channel	small conductance, Ca^{2+}-activated potassium channel

References

1. Makita N, Yagihara N, Crotti L, Johnson CN, Beckmann BM, Roh MS, Shigemizu D, Lichtner P, Ishikawa T, Aiba T, et al. Novel calmodulin mutations associated with congenital arrhythmia susceptibility. Circ Cardiovasc Genet. 2014;7:466–474. [PubMed: 24917665]
2. Crotti L, Johnson CN, Graf E, De Ferrari GM, Cuneo BF, Ovadia M, Papagiannis J, Feldkamp MD, Rathi SG, Kunic JD, et al. Calmodulin mutations associated with recurrent cardiac arrest in infants. Circulation. 2013;127:1009–1017. [PubMed: 23388215]
3. Pipilas DC, Johnson CN, Webster G, Schlaepfer J, Fellmann F, Sekarski N, Wren LM, Ogorodnik KV, Chazin DM, Chazin WJ, et al. Novel calmodulin mutations associated with congenital long QT syndrome affect Ca^{2+} current in human cardiomyocytes. Heart Rhythm. 2016;13:2012–2019. [PubMed: 27374306]
4. Boczek NJ, Gomez-Hurtado N, Ye D, Calvert ML, Tester DJ, Kryshtal D, Hwang HS, Johnson CN, Chazin WJ, Loporcaro CG, et al. Spectrum and Prevalence of CALM1-, CALM2-, and CALM3-Encoded Calmodulin Variants in Long QT Syndrome and Functional Characterization of a Novel Long QT Syndrome-Associated Calmodulin Missense Variant, E141G. Circ Cardiovasc Genet. 2016;9:136–146. [PubMed: 26969752]
5. Gomez-Hurtado N, Boczek NJ, Kryshtal DO, Johnson CN, Sun J, Nitu FR, Cornea RL, Chazin WJ, Calvert ML, Tester DJ, et al. Novel CPVT-Associated Calmodulin Mutation in CALM3 (CALM3-A103V) Activates Arrhythmogenic Ca2+ Waves and Sparks. Circ Arrhythm Electrophysiol. 2016;9: pii: e004161. [PubMed: 27516456]
6. Yin G, Hassan F, Haroun AR, Murphy LL, Crotti L, Schwartz PJ, George AL, Satin J. Arrhythmogenic calmodulin mutations disrupt intracellular cardiomyocyte Ca^{2+} regulation by distinct mechanisms. J Am Heart Assoc. 2014;3:e000996. [PubMed: 24958779]
7. Reed GJ, Boczek NJ, Etheridge SP, Ackerman MJ. CALM3 mutation associated with long QT syndrome. Heart Rhythm. 2015;12:419–422. [PubMed: 25460178]
8. Nyegaard M, Overgaard MT, Søndergaard MT, Vranas M, Behr ER, Hildebrandt LL, Lund J, Hedley PL, Camm AJ, Wettrell G, et al. Mutations in calmodulin cause ventricular tachycardia and sudden cardiac death. Am J Hum Genet. 2012;91:703–712. [PubMed: 23040497]
9. Hwang HS, Nitu FR, Yang Y, Walweel K, Pereira L, Johnson CN, Faggioni M, Chazin WJ, Laver D, George AL Jr, et al. Divergent regulation of ryanodine receptor 2 Ca^{2+} release channels by arrhythmogenic human calmodulin missense mutants. Circ Res. 2014;114:1114–1124. [PubMed: 24563457]
10. Limpitikul WB, Dick IE, Joshi-Mukherjee R, Overgaard MT, George AL Jr, Yue DT. Calmodulin mutations associated with long QT syndrome prevent inactivation of cardiac L-type Ca^{2+} currents

and promote proarrhythmic behavior in ventricular myocytes. J Mol Cell Cardiol. 2014;74:115–124. [PubMed: 24816216]

11. Yu CC, Ko JS, Ai T, Tsai WC, Chen Z, Rubart M, Vatta M, Everett TH 4th, George AL Jr, Chen PS. Arrhythmogenic calmodulin mutations impede activation of small-conductance Ca^{2+}-activated K^+ current. Heart Rhythm. 2016;13:1716–1723. [PubMed: 27165696]
12. Søndergaard M, Tian X, Liu Y, Wang R, Chazin WJ, Chen SR, Overgaard MT. Arrhythmogenic Calmodulin Mutations Affect the Activation and Termination of Cardiac Ryanodine Receptor-mediated Ca^{2+} Release. J Biol Chem. 2015;290:26151–26162. [PubMed: 26309258]
13. Søndergaard MT, Sorensen AB, Skov LL, Kjaer-Sorensen K, Bauer MC, Nyegaard M, Linse S, Oxvig C, Overgaard MT. Calmodulin mutations causing catecholaminergic polymorphic ventricular tachycardia confer opposing functional and biophysical molecular changes. FEBS J. 2015;282:803–816. [PubMed: 25557436]
14. Knollmann BC, Chopra N, Hlaing T, Akin B, Yang T, Ettensohn K, Knollmann BE, Horton KD, Weissman NJ, Holinstat I, et al. Casq2 deletion causes sarcoplasmic reticulum volume increase, premature Ca^{2+} release, and catecholaminergic polymorphic ventricular tachycardia. J Clin Invest. 2006;116:2510–2520. [PubMed: 16932808]
15. Cerrone M, Colombi B, Santoro M, di Barletta MR, Scelsi M, Villani L, Napolitano C, Priori SG. Bidirectional ventricular tachycardia and fibrillation elicited in a knock-in mouse model carrier of a mutation in the cardiac ryanodine receptor. Circ Res. 2005;96:e77–82. [PubMed: 15890976]
16. Gade AR, Marx SO, Pitt GS. An interaction between the III-IV linker and CTD in NaV1.5 confers regulation of inactivation by CaM and FHF. J Gen Physiol. 2020;152: pii: e201912434. doi: 10.1085/jgp.201912434. [PubMed: 31865383]
17. Cheng H, Lederer WJ, Cannell MB. Calcium sparks: elementary events underlying excitation-contraction coupling in heart muscle. Science. 1993;262:740–744. [PubMed: 8235594]
18. Cerrone M, Noujaim SF, Tolkacheva EG, Talkachou A, O'Connell R, Berenfeld O, Anumonwo J, Pandit SV, Vikstrom K, Napolitano C, et al. Arrhythmogenic mechanisms in a mouse model of catecholaminergic polymorphic ventricular tachycardia. Circ Res. 2007;101:1039–1048. [PubMed: 17872467]
19. Chen B, Guo A, Gao Z, Wei S, Xie YP, Chen SR, Anderson ME, Song LS. In situ confocal imaging in intact heart reveals stress-induced Ca(2+) release variability in a murine catecholaminergic polymorphic ventricular tachycardia model of type 2 ryanodine receptor(R4496C+/−) mutation. Circ Arrhythm Electrophysiol. 2012;5:841–849. [PubMed: 22722659]
20. Dash R, Kadambi V, Schmidt AG, Tepe NM, Biniakiewicz D, Gerst MJ, Canning AM, Abraham WT, Hoit BD, Liggett SB, Lorenz JN, et al. Interactions between phospholamban and beta-adrenergic drive may lead to cardiomyopathy and early mortality. Circulation. 2001;103(6):889–896. [PubMed: 11171800]
21. Francis GS, Benedict C, Johnstone DE, Kirlin PC, Nicklas J, Liang CS, Kubo SH, Rudin-Toretsky E, Yusuf S. Comparison of neuroendocrine activation in patients with left ventricular dysfunction with and without congestive heart failure. A substudy of the Studies of Left Ventricular Dysfunction (SOLVD). Circulation. 1990;82:1724–1729. [PubMed: 2146040]
22. Qin W, Dion SL, Kutny PM, Zhang Y, Cheng AW, Jillette NL, Malhotra A, Geurts AM, Chen YG, Wang H. Efficient CRISPR/Cas9-Mediated Genome Editing in Mice by Zygote Electroporation of Nuclease. Genetics. 2015;200:423–430. [PubMed: 25819794]
23. Weiss S, Oz S, Benmocha A, Dascal N. Regulation of cardiac L-type Ca^{2+} channel CaV1.2 via the β-adrenergic-cAMP-protein kinase A pathway: old dogmas, advances, and new uncertainties. Circ Res. 2013;113:617–631. [PubMed: 23948586]
24. Tsien RW, Bean BP, Hess P, Lansman JB, Nilius B, Nowycky MC. Mechanisms of calcium channel modulation by beta-adrenergic agents and dihydropyridine calcium agonists. J Mol Cell Cardiol. 1986;18:691–710. [PubMed: 2427730]
25. Zhang XD, Coulibaly ZA, Chen WC, Ledford HA, Lee JH, Sirish P, Dai G, Jian Z, Chuang F, Brust-Mascher I, et al. Coupling of SK channels, L-type Ca2+ channels, and ryanodine receptors in cardiomyocytes. Sci Rep. 2018;8:4670. [PubMed: 29549309]

26. Wagner S, Dybkova N, Rasenack EC, Jacobshagen C, Fabritz L, Kirchhof P, Maier SK, Zhang T, Hasenfuss G, Brown JH, et al. Ca^{2+}/calmodulin-dependent protein kinase II regulates cardiac Na^{+} channels. J Clin Invest. 2006;116:3127–3138. [PubMed: 17124532]
27. Hegyi B, Bányász T, Izu LT, Belardinelli L, Bers DM, Chen-Izu Y. β-adrenergic regulation of late Na^{+} current during cardiac action potential is mediated by both PKA and CaMKII. J Mol Cell Cardiol. 2018;123:168–179. [PubMed: 30240676]
28. Mustroph J, Maier LS, Wagner S. CaMKII regulation of cardiac K channels. Front Pharmacol. 2014;5:20. [PubMed: 24600393]
29. Sun J, MacKinnon R. Cryo-EM structure of a KCNQ1/CaM complex reveals insights into congenital long QT syndrome. Cell. 2017;169:1042–1050. [PubMed: 28575668]
30. Saito T, Ciobotaru A, Bopassa JC, Toro L, Stefani E, Eghbali M. Estrogen contributes to gender differences in mouse ventricular repolarization. Circ Res. 2009;105:343–352. [PubMed: 19608983]
31. Edwards AG, Grandi E, Hake JE, Patel S, Li P, Miyamoto S, Omens JH, Heller Brown J, Bers DM, McCulloch AD. Nonequilibrium reactivation of Na+ current drives early afterdepolarizations in mouse ventricle. Circ Arrhythm Electrophysiol. 2014;7:1205–1013. [PubMed: 25236710]
32. Gao Z, Rasmussen TP, Li Y, Kutschke W, Koval OM, Wu Y, Wu Y, Hall DD, Joiner ML, Wu XQ, et al. Genetic inhibition of Na^{+}/Ca^{2+} exchanger current disables fight or flight sinoatrial node activity without affecting resting heart rate. Circ Res. 2013;112:309–317. [PubMed: 23192947]
33. Maltsev AV, Yaniv Y, Stern MD, Lakatta EG, Maltsev VA. RyR-NCX-SERCA local cross-talk ensures pacemaker cell function at rest and during the fight-or-flight reflex. Circ Res. 2013;113:e94–e100. [PubMed: 24158576]
34. Berchtold MW, Zacharias T, Kulej K, Wang K, Torggler R, Jespersen T, Chen JN, Larsen MR, la Cour JM. The Arrhythmogenic Calmodulin Mutation D129G Dysregulates Cell Growth, Calmodulin-dependent Kinase II Activity, and Cardiac Function in Zebrafish. J Biol Chem. 2016;291:26636–26646. [PubMed: 27815504]
35. Lei M, Jones SA, Liu J, Lancaster MK, Fung SSM, Dobrzynski H, Camelliti P, Maier SKG, Noble D, Boyett MR. Requirement of neuronal- and cardiac-type Na^{+} channels for murine sinoatrial node pacemaking. J Physiol. 2004;559:835–848. [PubMed: 15254155]
36. Reddy Chichili VP, Xiao Y, Seetharaman J, Cummins TR, Sivaraman J. Structural basis for the modulation of the neuronal voltage-gated Na+ channel NaV1.6 by calmodulin. Sci Rep. 2013;3:2435–2442. [PubMed: 23942337]
37. Mitchell GF, Jeron A, Koren G. Measurement of heart rate and Q-T interval in the conscious mouse. Am J Physiol. 1998;274:H747–751. [PubMed: 9530184]
38. van der Werf C, Kannankeril PJ, Sacher F, Krahn AD, Viskin S, Leenhardt A, Shimizu W, Sumitomo N, Fish FA, Bhuiyan ZA, et al. Flecainide therapy reduces exercise-induced ventricular arrhythmias in patients with catecholaminergic polymorphic ventricular tachycardia. J Am Coll Cardiol. 2011;57:2244–2254. [PubMed: 21616285]
39. Maruyama M, Li BY, Chen H, Xu X, Song LS, Guatimosim S, Zhu W, Yong W, Zhang W, Bu G, et al. FKBP12 is a critical regulator of the heart rhythm and the cardiac voltage-gated sodium current in mice. Circ Res. 2011;108:1042–1052. [PubMed: 21372286]
40. Anumonwo JM, Tallini YN, Vetter FJ, Jalife J. Action potential characteristics and arrhythmogenic properties of the cardiac conduction system of the murine heart. Circ Res. 2001;89:329–335. [PubMed: 11509449]
41. Pallante BA, Giovannone S, Fang-Yu L, Zhang J, Liu N, Kang G, Dun W, Boyden PA, Fishman GI. Contactin-2 expression in the cardiac Purkinje fiber network. Circ Arrhythm Electrophysiol. 2010;3:186–194. [PubMed: 20110552]
42. Satoh H, Delbridge LM, Blatter LA, Bers DM. Surface:volume relationship in cardiac myocytes studied with confocal microscopy and membrane capacitance measurements: species-dependence and developmental effects. Biophys J. 1996;70:1494–1504. [PubMed: 8785306]
43. Picht E, Zima AV, Blatter LA, Bers DM. SparkMaster: automated calcium spark analysis with ImageJ. Am J Physiol Cell Physiol. 2007;293:C1073–C1081. [PubMed: 17376815]

Clinical Perspective

What Is New?

- Knock-in mice heterozygous for the p.Asn98Ser mutation in the *Calm1* gene encoding calmodulin exhibit sinus bradycardia, QT_c interval prolongation and catecholaminergic, bidirectional ventricular tachycardia.
- β-adrenergic receptor activation-induced increase in 'late' *L*-type calcium current contributes to the long QT phenotype.
- Pause-dependent early and delayed afterdepolarizations originating in the His-Purkinje network and working ventricular myocytes, respectively, are involved in the initiation and/or maintenance of catecholaminergic arrhythmias in knock-in mice.

What Are the Clinical Implications?

- Our results suggest the ventricular myocyte late *L*-type calcium current as a potential target in long QT syndrome caused by calmodulin mutations.
- Anti-bradycardia pacing may constitute a viable approach to suppress arrhythmias triggered by afterdepolarizations.

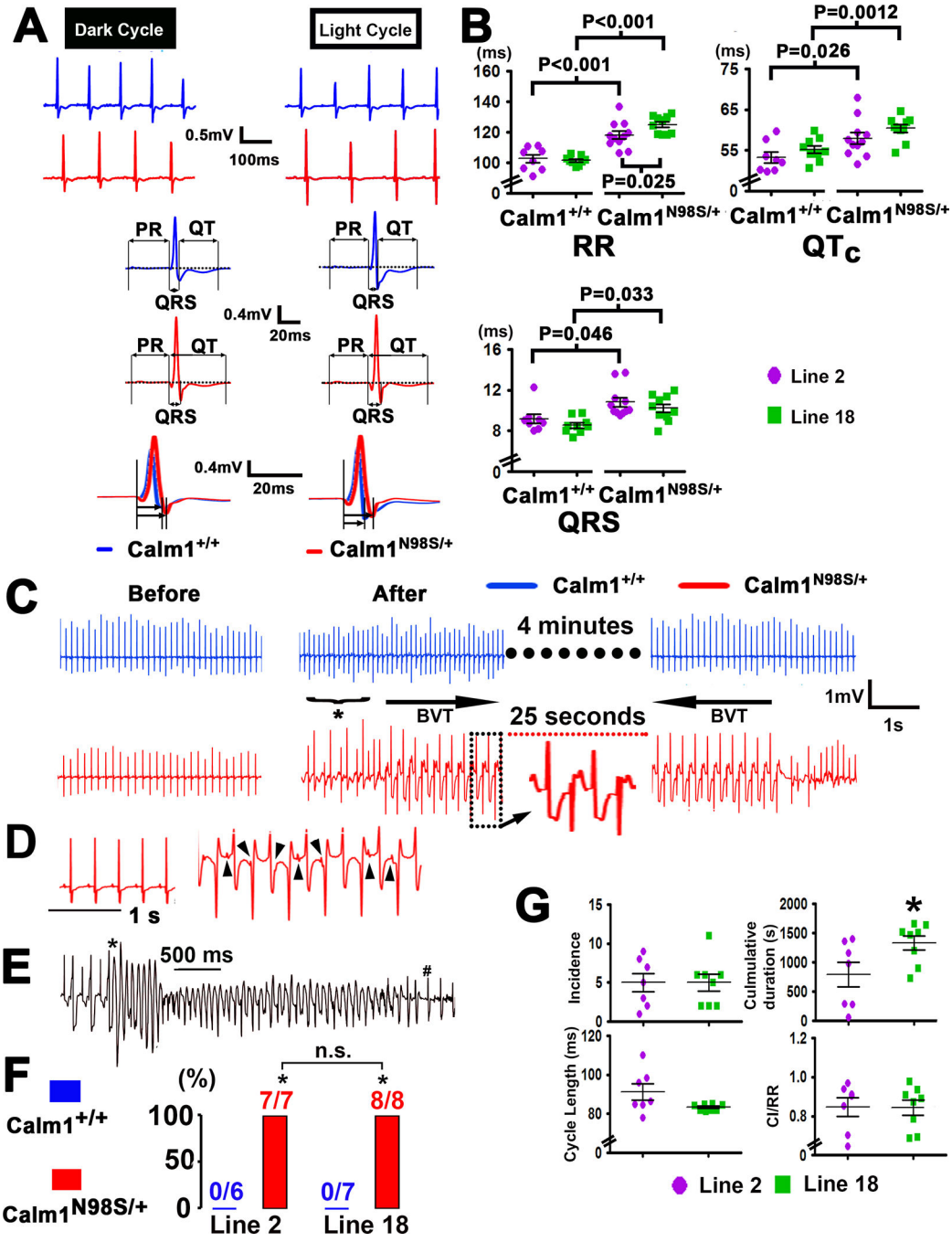

Figure 1. Calm1$^{N98S/+}$ mice exhibit sinus bradycardia, QRS widening, QT$_c$ prolongation and catecholaminergic ventricular tachycardia.

A, Top two rows show representative ECG traces recorded during the dark and light cycle in a littermate control (blue) and a Calm1$^{N98S/+}$ mouse (red) from line 2. Traces in the third and fourth row show signal-averaged ECGs obtained by overlaying all consecutive cycles recorded within a 5- to 10-s interval, using QRS maximum or QRS minimum for the alignment. Lower row shows superimposed QRS complexes at expanded time scales. **B**, Dot plots of RR, QRS and QT$_c$ intervals from littermate Calm1$^{+/+}$ and Calm1$^{N98S/+}$ mice of line

2 and line 18. Each dot represents the 24-h average in a single animal. Horizontal lines superimposed on dots depict mean and SEM. *P* values by *One Way ANOVA* followed by Student-Newman-Keuls Method for multiple comparisons (RR and QT_c) or *Kruskal-Wallis One Way ANOVA on Ranks* followed by *Dunn's Method* for multiple comparisons (QRS). Line 2: 8 $Calm1^{+/+}$and 11 $Calm1^{N98S/+}$mice; Line 18: 9 $Calm1^{+/+}$ and 10 $Calm1^{N98S/+}$ mice. **C**, $Calm1^{N98S/+}$ mice display bidirectional ventricular tachycardia (BVT). Representative telemetric ECG recordings from a conscious $Calm1^{+/+}$ and $Calm1^{N98S/+}$ mouse obtained before and shortly after intraperitoneal injection of epinephrine (2 mg per kg body weight) and caffeine (120 mg per kg body weight). In the $Calm1^{N98S/+}$ mouse, an episode of sustained BVT was preceded by ventricular bigeminy (*) and spontaneously reverted to sinus rhythm. No ventricular arrhythmias were observed in the $Calm1^{+/+}$ mouse. **D**, Complete dissociation of P waves (arrowheads) from QRS complexes during an episode of induced BVT. **E**, Polymorphic ventricular tachycardia in a male $Calm1^{N98S/+}$ mouse. * marks transition from BVT into polymorphic VT and # denotes conversion to sinus rhythm. **F**, Prevalence of sustained (>15 s) BVT induced by co-administration of epinephrine and caffeine. * $P < 0.001$ versus $Calm1^{+/+}$ by *Fisher's Exact* test. **G**, Incidence, cumulative duration, cycle length and CI/RR ratio of episodes of sustained (≥ 15 s) BVT during a 30-min period of post-injection telemetric ECG recordings in conscious $Calm1^{N98S/+}$ mice from line 2 and line 18. Dot plots with mean ± SEM shown as horizontal lines. N = 7, line 2; N = 8, line 18; *P=0.041 by *t* test. VT indicates ventricular tachycardia. CI indicates coupling interval and RR indicates RR interval.

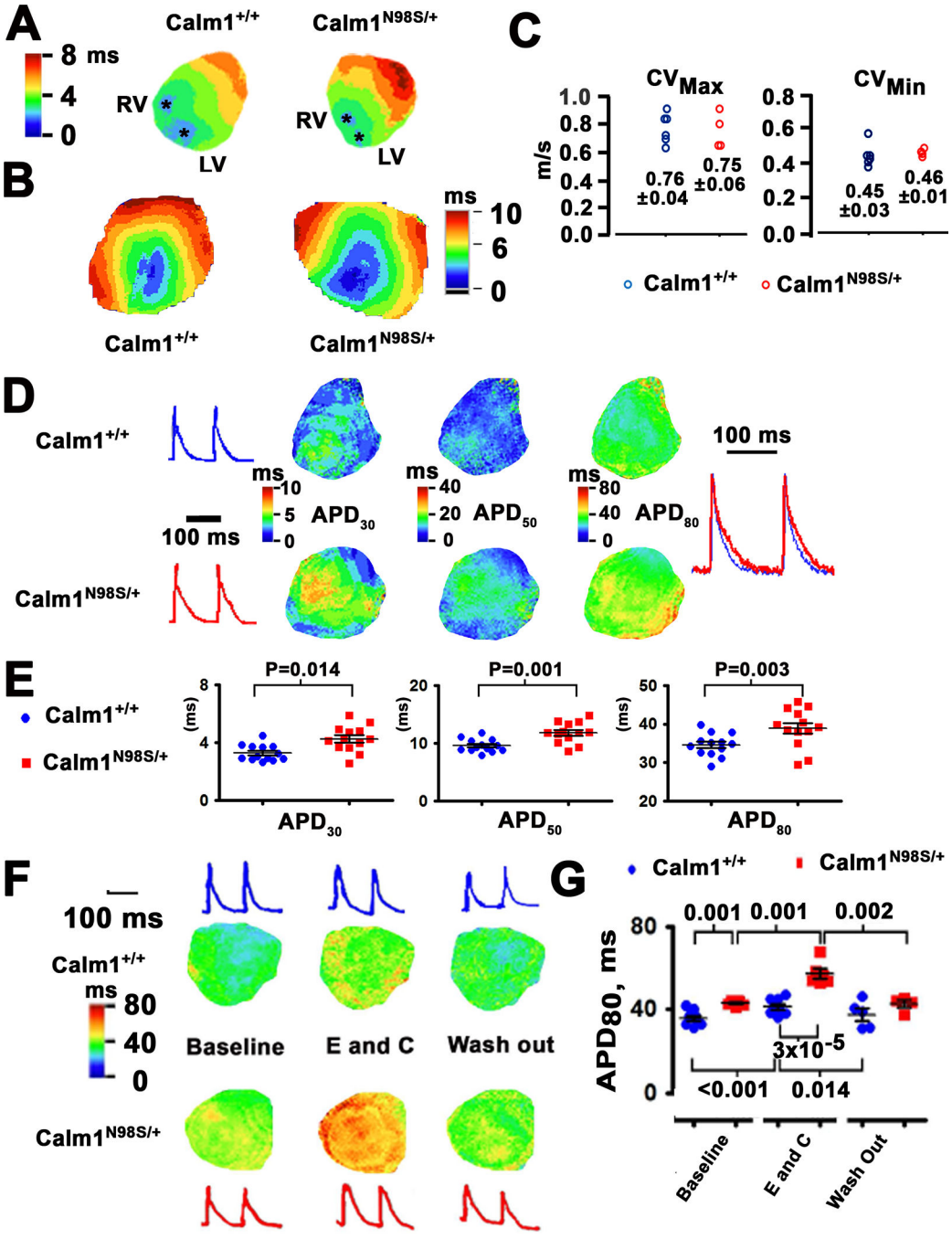

Figure 2. Delayed repolarization in ventricles of Calm1$^{N98S/+}$ mice.

A, Isochrone maps of epicardial activation during atrial pacing at a cycle length of 120 ms. Asterisks denote epicardial breakthrough sites on the anterior surface near the apex of the left (LV) and right ventricle (RV). Depolarization spread from the apex to the base. Sequential depolarizations are depicted in different colors according to the color legend shown in the left. Isochronal lines are 1 ms apart. **B**, Epicardial ventricular conduction velocities. Ventricular activation isochrone maps of the anterior aspect of a Calm1$^{+/+}$ and Calm1$^{N98S/+}$ heart. The anisotropic propagation in the ventricle enables measurements of

maximal and minimal conduction velocities (CV_{max} and CV_{min}). **C**, Dot plots of CVs. Numbers indicate mean and SEM in m/s from 6 $Calm1^{+/+}$ and 4 $Calm1^{N98S/+}$ hearts. No statistically significant differences between the two genotypes were found. **D**, Left: Representative optical action potentials from the anterior left ventricular epicardium of littermate $Calm1^{+/+}$ and $Calm1^{N98S/+}$ mice during atrial pacing at a cycle length of 120 ms. Middle three panels: exemplar maps of the repolarization time points at APD_{30}, APD_{50} and APD_{80}. Colored scale bars are shown in the inserts. Right: superimposition of the same optical action potentials shown in the left panels. **E**, Dot plots showing APD_{30}, APD_{50} and APD_{80} of littermate control and $Calm1^{N98S/+}$ mice. Black horizontal lines depict mean ± SEM. * $P \leq 0.02$ by *t*-test. N = 11 per genotype. **F**, Exacerbation of long QT phenotype upon exposure to epinephrine (E) and caffeine (C) combined. Exemplar ventricular repolarization (APD_{80}) isochrone maps of the anterior aspect of a $Calm1^{+/+}$ and a $Calm1^{N98S/+}$ heart at baseline, during E and C exposure, and following washout. Pacing cycle length, 120 ms. **G**, Scatter plots of APD_{80}. Black lines are mean ± SEM from 8 $Calm1^{+/+}$ and 6 $Calm1^{N98S/+}$ hearts. *P* values by *Repeated Measures ANOVA* followed by *Tukey* test for intragroup analyses; for intergroup analyses, a *t*-test (for comparisons at baseline and during washout) and *Mann-Whitney Rank Sum* test (for comparison during epinephrine) were used.

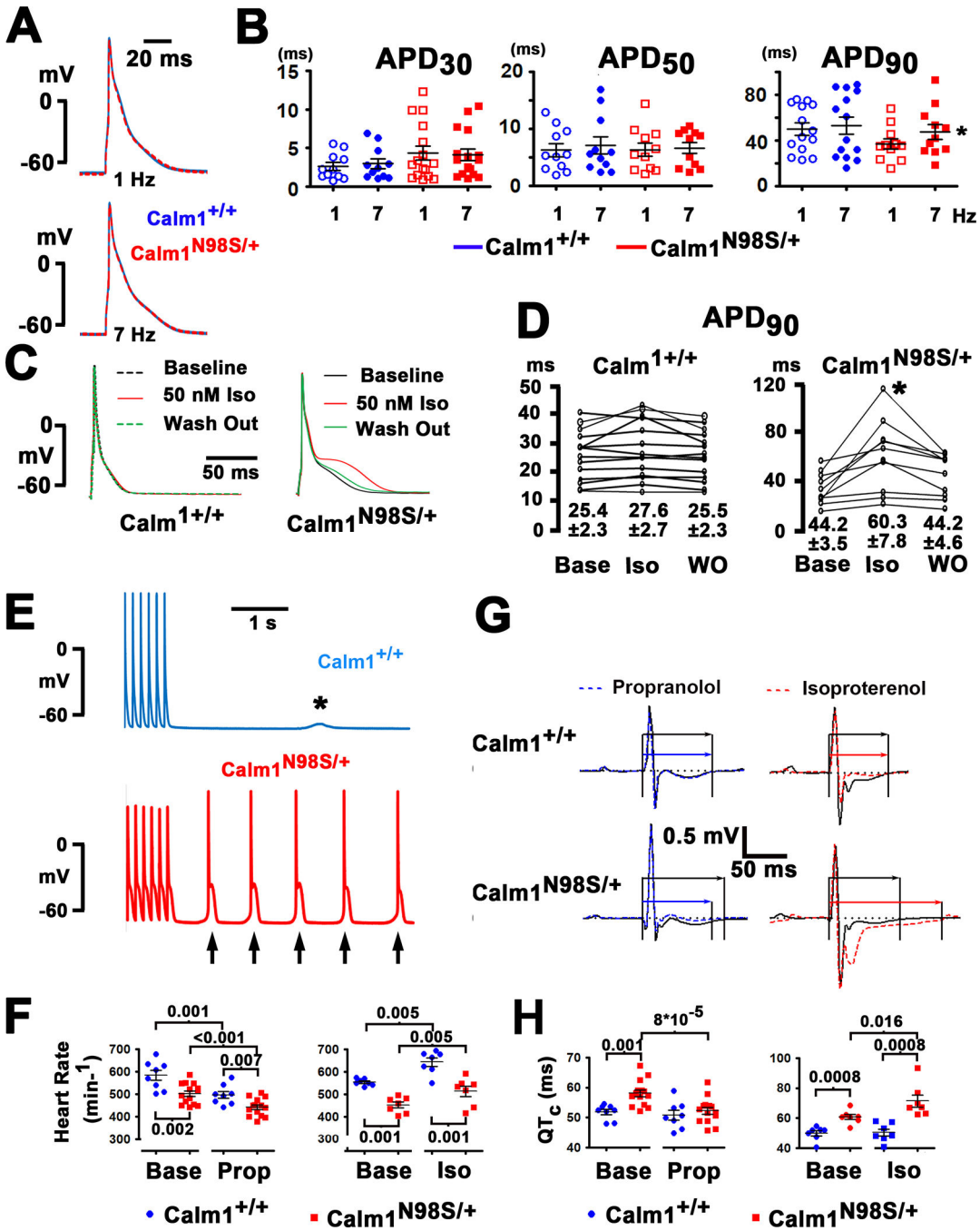

Figure 3. β-adrenergic stimulation induces a long QT phenotype in Calm1$^{N98S/+}$ mice.

A, Left panels: superimpositions of representative action potentials electrically recorded from single myocytes isolated from the left ventricular free wall of a Calm1$^{+/+}$ (blue) and a Calm1$^{N98S/+}$ (red) heart. Cells were paced at 1 and 7 Hz. Right panels: single action potentials at 1 and 7 Hz pacing at expanded time scales. **B**, Dot plots of APD_{30}, APD_{50} and APD_{90} in single ventricular myocytes paced at 1 and 7 Hz. Black lines denote mean ± SEM; 11 cells each from 3 Calm1$^{+/+}$ mice and from 4 Calm1$^{N98S/+}$ mice. * $P = 0.004$ vs. Calm1$^{N98S/+}$ 1 Hz by paired *t*-test. **C**, Superimpositions of representative action potentials

recorded from a $Calm1^{+/+}$ and a $Calm1^{N98S/+}$ ventricular myocyte at baseline, during isoproterenol (50 nM; Iso) treatment, and during washout. Action potentials were evoked by 2-ms square current injections delivered at 1 Hz**. D**, Summary of the effect of isoproterenol (Iso) on APD_{90} in $Calm1^{+/+}$ and $Calm1^{N98S/+}$ ventricular myocytes; 14 cells from 5 $Calm1^{+/+}$ mice and 10 cells from 4 $Calm1^{N98S/+}$ mice. * $P < 0.01$ by *Repeated Measures ANOVA* followed by *Tukey* test for pairwise multiple comparisons. Numbers denote mean ± SEM in ms. Base: baseline. **E**, Original recordings of a delayed afterdepolarization (*) and delayed afterdepolarization-triggered action potentials (arrows) in a $Calm1^{+/+}$ and a $Calm1^{N98S/+}$ ventricular cardiomyocyte, respectively. Traces show the terminal 6 paced action potentials from a 10-s train at 7 Hz in the presence of 50 nM isoproterenol. **F**, Summary of the effects of propranolol (1 mg/kg) or isoproterenol (0.17 mg/kg) on heart rate. Horizontal black lines denote mean ± SEM. Propranolol (Prop): N = 8, $Calm1^{+/+}$ mice; N = 14, $Calm1^{N98S/+}$ mice. Isoproterenol (Iso): N = 7, $Calm1^{+/+}$; N = 7, $Calm1^{N98S/+}$. *P* values by unpaired and paired *t*-test. Base: baseline. **G**, Representative QT interval changes in conscious male $Calm1^{+/+}$ and $Calm1^{N98S/+}$ mice following intraperitoneal injection of propranolol (1 mg/kg) or isoproterenol (0.17 mg/kg). Shown are signal-averaged ECGs obtained by overlaying all consecutive cycles recorded within a 5- to 10-s interval, ca. 20 min after injection. Arrows mark QT intervals. **H**, Summary of the effects of propranolol and isoproterenol on QT_c interval. Horizontal black lines denote mean ± SEM. Propanolol (Prop): N = 8, $Calm1^{+/+}$ mice; N = 14, $Calm1^{N98S/+}$ mice. Isoproterenol (Iso): N = 7, $Calm1^{+/+}$; N = 7, $Calm1^{N98S/+}$. *P* values by unpaired and paired *t*-test. Base: baseline.

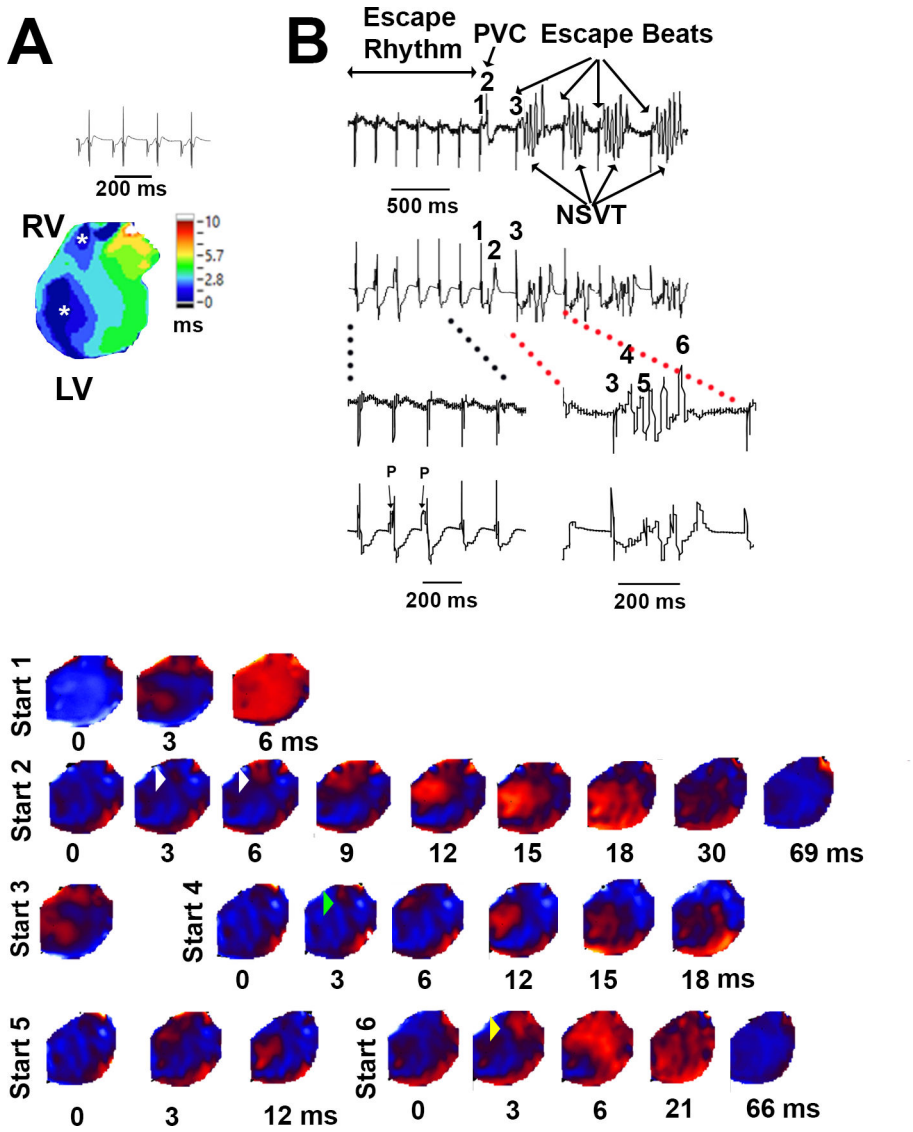

Figure 4. Ventricular arrhythmia in a Calm1$^{N98S/+}$ heart.

A, Volume-conducted ECG and epicardial activation map in sinus rhythm. Asterisks denote concentric breakthroughs on the anterior right and left ventricular free walls. **B**, Volume-conducted ECGs and epicardial voltage maps in the presence of 100 nM isoproterenol and 3.6 mmol/L extracellular Ca^{2+}. QRS complex numbers on ECG correspond to voltage map sequences with the same numbers. The ECG shows a junctional escape rhythm with AV dissociation and a QRS morphology similar to that during SR, a single premature ventricular complex (PVC) and 4 episodes of non-sustained VT (NSVT). Maps show epicardial breakthrough pattern during junctional escape rhythm (sequence #1), RV focal discharge (white arrowheads) coinciding with the emergence of an R-on-T ectopic ventricular beat (sequence #2) in the ECG, RV focal discharge (green arrowhead) initiating NSVT with a large wave front traveling across the epicardial surface (sequences #3 - #5), followed by an RV focal discharge (yellow arrowhead) coinciding with the last beat of the arrhythmia episode (sequence #6). Map sequences of the other 3 VT episodes similarly showed RV

focal discharges initiating NSVT. Times denote intervals after the onset of epicardial breakthroughs.

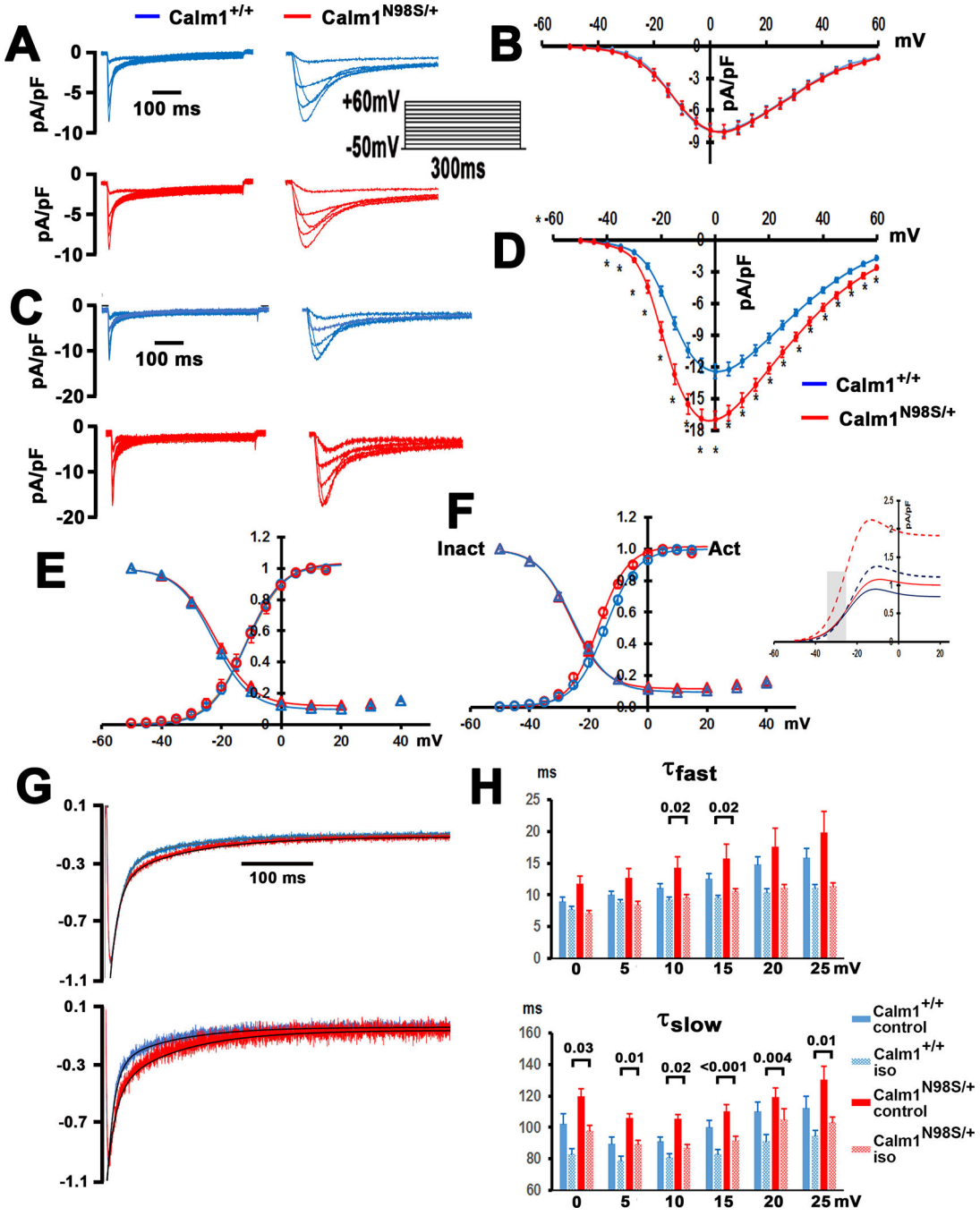

Figure 5. Calm1^{N98S} heterozygosity potentiates β-adrenergic receptor-mediated effects on cardiac $I_{Ca.L}$.

A and **C**, Exemplar whole-myocyte $I_{Ca.L}$ traces evoked by 300-ms step depolarizations to voltages from −50 to +60 mV from a holding potential of −70 mV in control (A) and during exposure to isoproterenol (C). Interpulse interval was 5 s. Top: voltage-clamp protocol. **B** and **D**, Peak $I_{Ca.L}$ density – voltage relations in Calm1$^{+/+}$ and Calm1$^{N98S/+}$ ventricular myocytes in the absence (B) and presence of isoproterenol (D). Values are mean ± SEM. Control: 11 cells each from 5 Calm$^{+/+}$ mice and 5 Calm1$^{N98S/+}$ mice. Isoproterenol: 24 cells

from 5 $Calm1^{+/+}$ mice and 29 cells from 5 $Calm1^{N98S/+}$ mice. * $P < 0.03$ versus $Calm1^{+/+}$ by *t*-test. **E** and **F**, Voltage-dependence of steady-state $I_{Ca.L}$ activation and inactivation in the absence (E) and presence (F) of isoproterenol (50 nM). Values are mean ± SEM. Solid lines are best fits of the data to a Boltzmann function (fit parameters in Supplemental Table 6). Half-activation voltage in the presence of isoproterenol was significantly more negative in $Calm1^{N98S/+}$ versus $Calm1^{+/+}$ myocytes (−16.8 ± 0.8 mV versus −13.9 ± 0.8 mV; $P = 0.018$ by *t*-test). Insert: Calculation of the predicted window $I_{Ca.L}$ density as a function of voltage. Amplitude of window $I_{Ca.L}$ density was estimated as SS-act x SS-inact x $I_{Ca.L}$ (at V_{peak}). Shaded area marks the range of membrane potential typically occurring during the action potential plateau of isoproterenol-treated $Calm1^{N98S/+}$ ventricular myocytes. SS-act and SS-inact indicate steady state activation and steady state inactivation, respectively. **G**, Exemplar whole-myocyte $I_{Ca.L}$ traces elicited by 300-ms step depolarizations to +10 mV in the absence (top) and presence of 50 nM isoproterenol (bottom). Solid black lines are best fits of $I_{Ca.L}$ decay to a double exponential: $y(t) = A_{fast} \exp(-t/\tau_{fast}) + A_{slow} \exp(-t/\tau_{slow}) + y_0$. **H**, Summary of $I_{Ca.L}$ inactivation time constants, τ_{fast} and τ_{slow}, as a function of test potential. Values are mean ± SEM. Control: 11 cells from 5 $Calm1^{+/+}$ mice and 12 cells from 4 $Calm1^{N98S/+}$ mice; isoproterenol: 23 cells from 5 $Calm1^{+/+}$ mice and 25 cells from 6 $Calm1^{N98S/+}$ mice. Numbers above brackets indicate *P* values by *One way ANOVA* followed by multiple comparisons using the *Bonferroni t*-test (for τ_{slow} at 10 and 25 mV) or *Kruskal Wallis One Way ANOVA on Ranks* followed by *Dunn's Method* for multiple comparisons (for all other voltages).

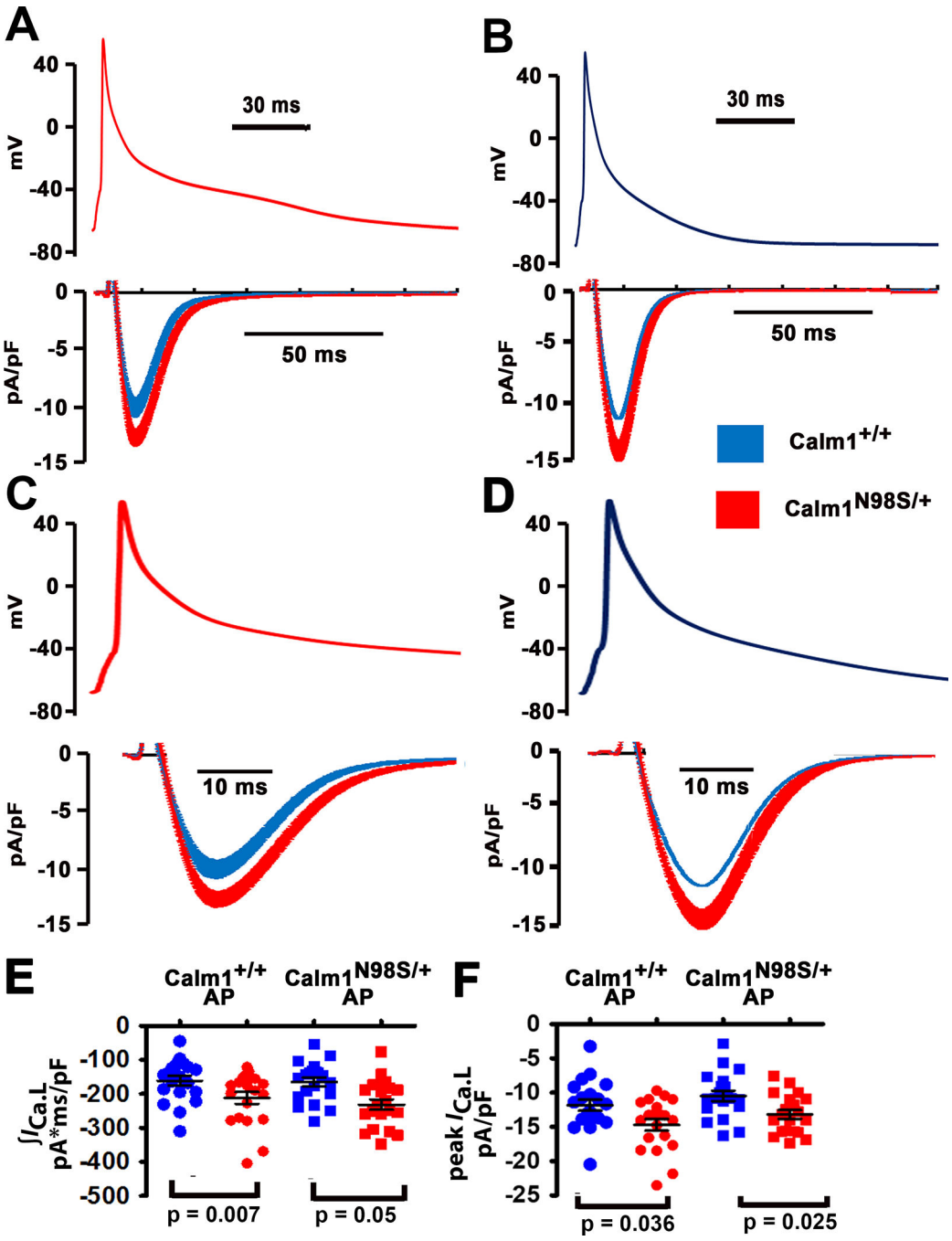

Figure 6. β-adrenergic receptor stimulation enhances peak and late $I_{Ca.L}$ during the action potential in Calm1$^{N98S/+}$ ventricular myocytes.

A and **B,** L-type Ca^{2+} currents (lower panels) elicited by "typical" action potential waveforms (upper panels) that had been pre-recorded from isoproterenol (50 nM) - treated Calm1$^{+/+}$ and Calm1$^{N98S/+}$ ventricular myocytes. Action potential waveforms were delivered at 1 Hz steady-state frequency in the presence of isoproterenol (50 nM). Each data point in an $I_{Ca.L}$ trace represents the mean ± SEM of 20 and 22 cells isolated from 4 Calm1$^{+/+}$ and 4 Calm1$^{N98S/+}$ hearts, respectively. **C** and **D**, The same action potential

waveforms and $I_{Ca.L}$ traces shown in A and B at expanded time scales. **E** and **F**, Dot plots of total $I_{Ca.L}$ ($\int I_{Ca.L}$; E) normalized to cell capacitance and peak $I_{Ca.L}$ density during the ventricular action potential in isoproterenol-treated cardiomyocytes. AP: action potential. Horizontal lines indicate mean ± SEM; 20 cells from 4 $Calm1^{+/+}$ mice and 22 cells from 4 $Calm1^{N98S/+}$ mice. *P* values by *ANOVA* followed by *Bonferroni* test for *post hoc* comparison.

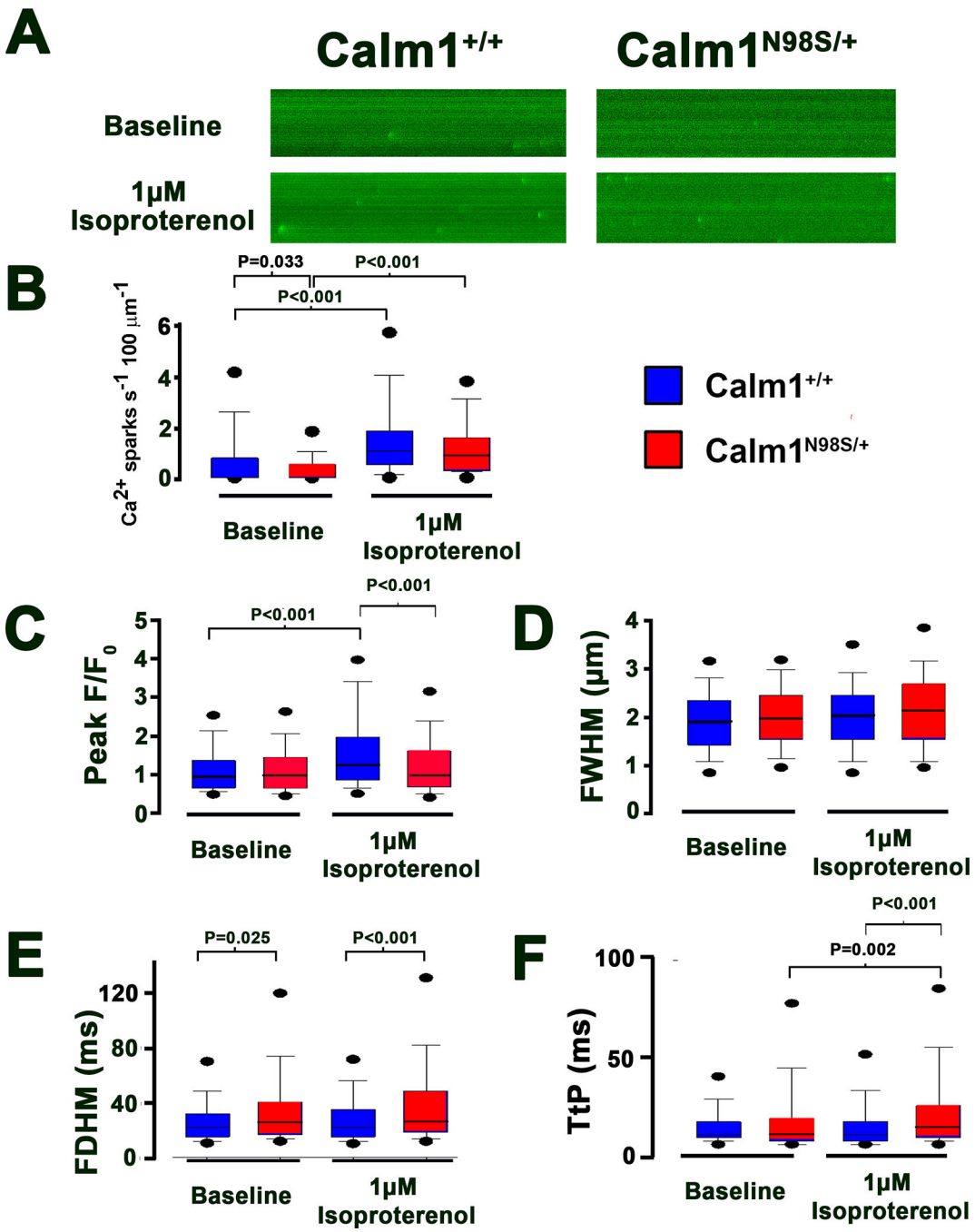

Figure 7. Resting Ca^{2+} spark properties in $Calm1^{+/+}$ and $Calm1^{N98S/+}$ ventricular myocytes.

A, Confocal line-scan images of diastolic Ca^{2+} sparks recorded in a $Calm1^{+/+}$ and a $Calm1^{N98S/+}$ cell in the absence (top) and presence (bottom) of 1 μM isoproterenol. **B,** Box and whisker plots of (B) Ca^{2+} spark occurrence, (C) spark amplitude, (D) full width at half maximum (FWHM), (E) full duration at half maximum (FDHM), and (F) time to peak (TtP). The ends of the box are the upper and lower quartiles. The medians are marked by the horizontal lines inside the boxes, whereas the whiskers extend to the 10% and 90% quartiles. Black dots mark 5% and 95% percentiles. Numbers above horizontal lines denote *P* values

by *Kruskal-Wallis One Way ANOVA on Ranks* followed by pairwise comparisons using *Dunn's* method; $Calm1^{+/+}$: 443 sparks in 127 cells from 11 hearts without isoproterenol, 546/32/5 with 1 μM isoproterenol; $Calm1^{N98S/+}$: 274/125/9 without isoproterenol, 517/37/4 with 1 μM isoproterenol.

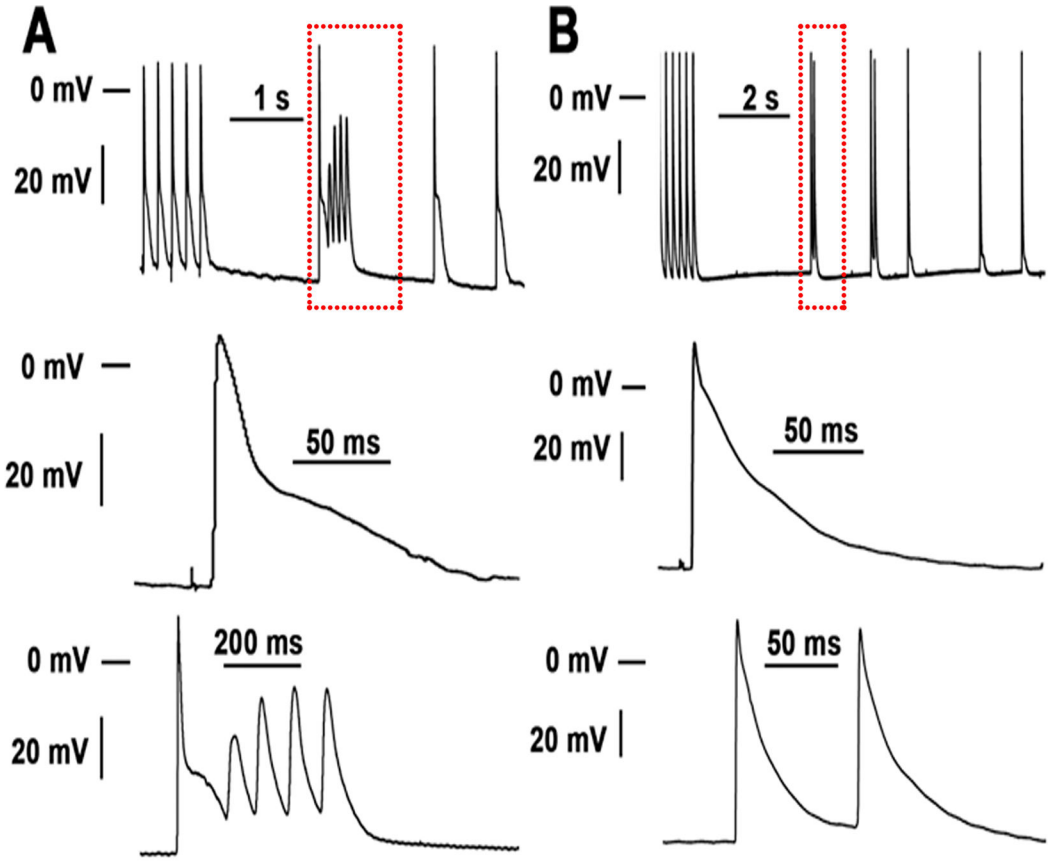

C

	Calm1$^{+/+}$	Calm1$^{N98S/+}$
	N = 10; n = 55	N = 10; n = 67
Number of conduction fibers with EADs	6	34 *
Number of wedges with EADs	4	10
Take-off potential, mV	-60.8 ± 5.6	-52.4 ± 12.6
EAD amplitude, mV	34.1 ± 35.6	27.8 ± 29.9
Diastolic interval, ms	616 ± 202	1166 ± 824 #

Figure 8. Pause-dependent early afterdepolarizations in the His-Purkinje network of Calm1$^{N98S/+}$ hearts.

A and **B** Top: original traces of membrane potential obtained from His-Purkinje myocytes in Calm1$^{N98S/+}$ hearts. The traces shown include the last 5 action potentials from a train of 30 action potentials at 5 Hz pacing, followed by >1-s pauses and spontaneous action potentials. Middle: Magnified views of the final paced action potential. Bottom: Magnified views of the boxed regions in the top panels, illustrating pause-dependent repetitive early afterdepolarizations (A) and an early afterdepolarization (B) arising from a spontaneous action potential. Neither cell developed diastolic (delayed) afterdepolarizations. Note the

presence of automaticity in the fiber shown in B. **C**, Properties of early afterdepolarizations. N and n are the number of hearts and conduction fibers, respectively. EAD, early afterdepolarization; mean values for take-off potential, EAD amplitude and diastolic interval preceding the EAD-containing cycle were averaged from 202 and 23 EADs in $Calm1^{N98S/+}$ and $Calm1^{+/+}$ wedges, respectively. * $P < 0.001$ versus $Calm1^{+/+}$ by *Chi-square* test. # $P = 0.006$ versus $Calm1^{+/+}$ by *Mann-Whitney Rank Sum* test.